INTERNATIONAL JOURNAL FOR NUMERICAL METHODS IN ENGINEERING
*Int. J. Numer. Meth. Engng* 2006; **66**:1514–1546
Published online 11 April 2006 in Wiley InterScience (www.interscience.wiley.com). DOI: 10.1002/nme.1698

# The Characteristic-Based Split (CBS) scheme—a unified approach to fluid dynamics

P. Nithiarasu[1,*,†], R. Codina[2,‡] and O. C. Zienkiewicz[1,§]

[1]*Civil and Computational Engineering Centre, School of Engineering, University of Wales Swansea, Swansea SA2 8PP, U.K.*
[2]*Universitat Politécnica de Catalunya, Jordi Girona 1-3, 08034 Barcelona, Spain*

SUMMARY

This paper presents a comprehensive overview of the characteristic-based methods and Characteristic-Based Split (CBS) scheme. The practical difficulties of employing the original characteristic schemes are discussed. The important features of the CBS scheme are brought out by studying several problems of compressible and incompressible flows. All special consideration necessary for solving these problems are thoroughly discussed. The CBS scheme is presented in such a way that any interested researcher should be able to develop a code using the information provided. Several invicid and viscous flow examples are also provided to demonstrate the unified CBS approach. For sample two-dimensional codes, input files and instructions, the readers are referred to 'www.nithiarasu.co.uk' Copyright © 2006 John Wiley & Sons, Ltd.

KEY WORDS: characteristic Galerkin; CBS scheme; compressible and incompressible flows; explicit and semi-implicit schemes

## 1. INTRODUCTION

Since its introduction in 1995 [1, 2], the CBS scheme has been widely employed by the authors and several other researchers for solving fluid and solid dynamic problems. It is however, important to mention here that its full potential is yet to be realized. In this article, we provide an overview of the method and summarize the developments that took place over the last ten years.

Stabilized schemes for compressible and incompressible flows need to have sufficient stability to suppress oscillations due to standard Galerkin discretization of the convection terms. A number of stabilizing schemes have been introduced over the last twenty years [3–15]. Among these, the characteristic-based schemes and Taylor–Galerkin schemes are developed

*Correspondence to: P. Nithiarasu, Civil and Computational Engineering Centre, School of Engineering, University of Wales Swansea, Swansea SA2 8PP, U.K.
†E-mail: P.Nithiarasu@swansea.ac.uk
‡E-mail: ramon.codina@upc.edu
§E-mail: O.C.Zienkiewicz@swansea.ac.uk

*Received 16 March 2005*
*Revised 7 June 2005*
*Accepted 2 February 2006*

using the time stepping as the basis. The use of characteristic Galerkin schemes has been demonstrated by several authors in the past for simple convection–diffusion problems [10–17] and recently these methods have been employed to deal with full fluid dynamics equation [18]. Although several versions of characteristic Galerkin schemes are possible, the simple characteristic Galerkin scheme based on a Taylor expansion is attractive due to its easy implementation and its equivalence with standard characteristic Galerkin schemes introduced by Morton and co-workers [11, 13]. Its equivalence to other standard stabilizing schemes can also be proved for convection–diffusion problems if the time step is suitably scaled using an appropriate velocity scale and a length scale. In addition to these advantages, the simple characteristic Galerkin scheme can be subjected to fully explicit form of solution [3].

Another difficulty, unique to the Navier–Stokes equations, is the instability created by the pressure term in the momentum equations. The requirement on the velocity-pressure interpolation to avoid this instability is often referred to as LBB condition. This condition is circumvented by many procedures as discussed in Reference [19]. However, the operator split or projection methods seem to be popular among the researchers dealing with incompressible material since it was introduced by Chorin [20] in 1967. The semi-, quasi- and fully-implicit forms of solution procedures are common in the incompressible fluid dynamics literature. However, the split method was not used for compressible fluid flow calculations until the method was introduced for non-conservation form of equations by Zienkiewicz and Wu [21]. In 1995 the split was introduced by Zienkiewicz and Codina [2] along with a Characteristic Galerkin approximation to solve the Navier–Stokes equations in its conservation form.

Although the original method was introduced for fully explicit form of solution procedure [22], later it was extended to semi-implicit form for both compressible and incompressible flows [23]. Several publications followed on the applications of the CBS scheme to compressible and incompressible flows [24–36]. Further extensions of the CBS scheme to shallow water flows [37, 38] and solid dynamics [39] were also carried out. The CBS scheme was also simultaneously extended to solve porous medium flows [40, 41].

From the beginning it was realized that the explicit solution to the fully incompressible fluid dynamics equations using the CBS scheme is not possible, unless an artificial compressibility method is employed. Recently, an artificial compressibility method was coupled with the explicit scheme to compute incompressible fluid flows efficiently [42, 43]. The true transient solution was achieved using a dual time stepping approach. Recently, the method was extended to solve visco-elastic flow problems [44]. Comparison of the CBS method against other standard stabilization methods is available in References [45, 46].

The last review of the CBS method was published in 1999 [28]. Rapid progress in terms of improvements in the algorithm and extension to several other engineering problems has been taking place in the last five years. Thus, we believe it is timely to review the CBS method again. We hope this paper and other papers appeared in this issue of the journal serve as a reference work on the CBS method.

## 2. CONVECTION–DIFFUSION PROBLEM

Let us consider the following simple scalar convection–diffusion equation:

$$\alpha \frac{\partial \phi}{\partial t} + \frac{\partial F_i}{\partial x_i} + \frac{\partial G_i}{\partial x_i} = 0 \tag{1}$$

 

or in non-conservation form with divergence free velocity field.

$$\alpha \frac{\partial \phi}{\partial t} + u_i \frac{\partial \phi}{\partial x_i} - \frac{\partial}{\partial x_i}\left(k \frac{\partial \phi}{\partial x_i}\right) = 0 \tag{2}$$

where $\alpha$ is a constant, $\phi$ is a scalar variable, $F_i$ is the convective flux, $G_i$ is the diffusive flux and $k$ is the diffusion coefficient. The problem statement is complete with the following boundary conditions:

$$\begin{aligned} &\phi = \overline{\phi} \quad \text{on } \Gamma_\phi \quad \text{and} \\ &q = \overline{q} \quad \text{on } \Gamma_f \end{aligned} \tag{3}$$

in which

$$\Gamma = \Gamma_\phi \cup \Gamma_f \tag{4}$$

and $q$ is the flux.

## 3. THE NAVIER–STOKES EQUATIONS

The generalized fluid dynamics equation in conservation form may be written as

*Mass conservation*

$$\frac{\partial \rho}{\partial t} = \frac{1}{c^2}\frac{\partial p}{\partial t} = -\frac{\partial U_i}{\partial x_i} \tag{5}$$

where $c$ is the speed of sound and depends on specific energy, $E$, pressure, $p$ and density, $\rho$ and, assuming constant entropy

$$c^2 = \frac{\partial p}{\partial \rho} = \frac{\gamma p}{\rho} \tag{6}$$

for an ideal gas. In Equation (6) $\gamma$ is the ratio of specific heats equal to $c_p/c_v$, where $c_p$ is the specific heat at constant pressure and $c_v$ is the specific heat at constant volume, and we define the mass flow flux as

$$U_i = \rho u_i \tag{7}$$

*Momentum conservation*

$$\frac{\partial U_i}{\partial t} = -\frac{\partial}{\partial x_j}(u_j U_i) + \frac{\partial \tau_{ij}}{\partial x_j} - \frac{\partial p}{\partial x_i} - \rho g_i \tag{8}$$

*Energy conservation*

$$\frac{\partial (\rho E)}{\partial t} = -\frac{\partial}{\partial x_i}(u_i \rho E) + \frac{\partial}{\partial x_i}\left(k \frac{\partial T}{\partial x_i}\right) - \frac{\partial}{\partial x_i}(u_i p) + \frac{\partial}{\partial x_i}(\tau_{ij} u_j) - \rho g_i u_i \tag{9}$$

In all of the above $u_i$ are the velocity components, $T$ is the absolute temperature, $\rho g_i$ represents body forces and other source terms, $k$ is the thermal conductivity, and $\tau_{ij}$ are the

 

deviatoric stress components given by

$$\tau_{ij} = \mu \left( \frac{\partial u_i}{\partial x_j} + \frac{\partial u_j}{\partial x_i} - \frac{2}{3} \delta_{ij} \frac{\partial u_k}{\partial x_k} \right) \tag{10}$$

where $\delta_{ij}$ is the Kronecker delta. In general, $\mu$, the dynamic viscosity, in the above equation is a function of temperature, $\mu(T)$, and appropriate relations will be used if necessary. The equations are completed by the universal gas law when the flow is coupled and compressible

$$p = \rho R T \tag{11}$$

where $R$ is the universal gas constant. The problem statement will be complete with the specification of appropriate boundary and initial conditions similar to the one defined in the previous section.

## 4. CHARACTERISTIC-BASED SCHEMES

The characteristic-based methods are widely employed in all areas of fluid dynamics. This section provides a background to these methods. We focus our attention towards three variants of characteristic methods and the relationship between them in the following subsections.

### *4.1. Direct Characteristic Galerkin method*

In order to understand the characteristic methods Figure 1 may be useful. This figure explains how the characteristics propagate in $x$–$t$ plane if a linear convection (zero diffusion in Equation (2)) equation is considered with a constant convection velocity in one dimension. From this figure we can write

$$\phi(y)^{n+1} = \phi(x)^n \tag{12}$$

This shows the well known fact that the variable propogated along a characteristic (characteristic variable) is constant irrespective of the time level at which the particle lies.

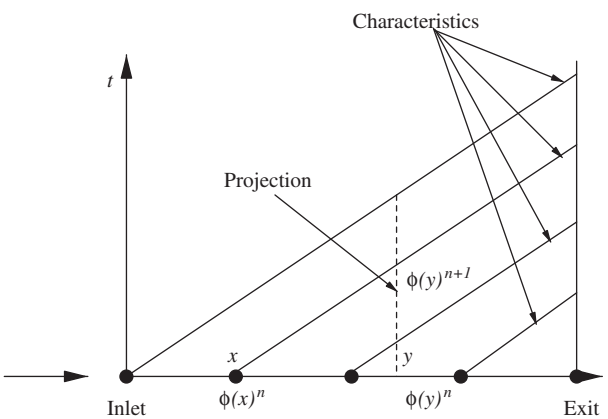


Figure 1. Linear convection problem. Characteristics.

 

In Equation (12) $y$ is the distance travelled by a particle at the speed of the characteristic, which is identical to the convection velocity for scalar problems. For a simple one-dimensional linear case this may be written as

$$y = x + u\Delta t \tag{13}$$

where $\Delta t$ is the time step and $x$ is referred to as the 'foot of the characteristic'.

Now, it is possible to weight Equation (12) and integrate over the domain. The weighting functions corresponding to either $x$ or at $y$ may be employed to develop the weighted residual form. We employ the weighting function at $y$ to form the weak form as

$$\int_\Omega \phi(y)^{n+1} w(y)\,\mathrm{d}\Omega = \int_\Omega \phi(x)^n w(y)\,\mathrm{d}\Omega \tag{14}$$

If the spatial approximation is employed along with the Galerkin weighting we will have

$$\int_\Omega N_i(y)\phi(y)_i^{n+1} N_j(y)\,\mathrm{d}\Omega = \int_\Omega N_i(x)\phi(x)_i^n N_j(y)\,\mathrm{d}\Omega \tag{15}$$

Evaluation of the LHS is simple for simplex elements via exact integration and will result in a positive definite, symmetric mass matrix. Since the $N_i(x)$ and $N_i(y)$ lie at different spatial positions (see Figure 1) exact integration is not possible. It is, however, possible to employ an approximate integration procedure. This integration needs to be carried out by back tracking the position $x$ at each time step. In one-dimensional flows this is not difficult but in multi-dimensional calculations involving complex geometries this procedure may not be the best option. To overcome the difficulties of the direct method, several alternatives were proposed and in the following sub-sections we consider two possible alternatives.

### *4.2. Indirect Characteristic Galerkin method*

The name indirect method is not necessarily universal. We adopt this terminology to represent method discussed by Morton, Donea and co workers [11, 15]. From Equation (12), a true solution satisfies the following identity:

$$\begin{aligned}\int_\Omega \phi(x)^{n+1} w(x)\,\mathrm{d}\Omega - \int_\Omega \phi(x)^n w(x)\,\mathrm{d}\Omega &= \int_\Omega \phi(y)^{n+1} w(y)\,\mathrm{d}\Omega - \int_\Omega \phi(x)^n w(x)\,\mathrm{d}\Omega \\ &= \int_\Omega \phi(x)^n w(y)\,\mathrm{d}\Omega - \int_\Omega \phi(x)^n w(x)\,\mathrm{d}\Omega \\ &= \int_\Omega \phi(x)^n [w(y) - w(x)]\,\mathrm{d}\Omega \end{aligned} \tag{16}$$

In the above equation $\phi(y)^{n+1} = \phi(x)^n$ is substituted, which is obvious from Figure 1. We can rewrite Equation (16) as

$$\int_\Omega \phi(x)^n [w(y) - w(x)]\,\mathrm{d}\Omega = \int_\Omega \phi(x)^n \frac{\mathrm{d}}{\mathrm{d}x}\left[\int_x^y w(z)\,\mathrm{d}z\right]\mathrm{d}\Omega \tag{17}$$

 

which, may be rewritten as

$$\int_\Omega \phi(x)^n \frac{\mathrm{d}}{\mathrm{d}x}\left[\int_x^y w(z)\,\mathrm{d}z\right]\mathrm{d}\Omega = -\int_\Omega \frac{\mathrm{d}}{\mathrm{d}x}\phi^n(x)\left[\int_x^y w(z)\,\mathrm{d}z\right]\mathrm{d}\Omega \tag{18}$$

If we introduce a modified weighting of the form

$$W^n = \frac{1}{u\Delta t}\int_x^{x+u\Delta t} w(z)\,\mathrm{d}z \tag{19}$$

into Equation (18) we get

$$-\int_\Omega \frac{\mathrm{d}}{\mathrm{d}x}\phi^n(x)\left[\int_x^y w(z)\,\mathrm{d}z\right]\mathrm{d}\Omega = -\Delta t\int_\Omega u^n \frac{\mathrm{d}}{\mathrm{d}x}\phi^n W^n\,\mathrm{d}\Omega \tag{20}$$

From Equations (16) and (20) we can write

$$\int_\Omega [\phi(x)^{n+1} - \phi(x)^n]w(x)\,\mathrm{d}\Omega = -\Delta t\int_\Omega u^n \frac{\mathrm{d}}{\mathrm{d}x}\phi^n W^n\,\mathrm{d}\Omega \tag{21}$$

For a linear element system the above form in one-dimensional problem gives [11]

$$\begin{aligned}\phi_i^{n+1} + \frac{1}{6}(\phi_{i-1}^{n+1} - 2\phi_i^{n+1} + \phi_{i+1}^{n+1}) = \phi_i^n + \frac{1}{6}(\phi_{i-1}^n - 2\phi_i^n + \phi_{i+1}^n)\\ - \frac{C}{2}(\phi_{i+1} - \phi_{i-1})^n\\ + \frac{C^2}{2}(\phi_{i-1} - 2\phi_i + \phi_{i+1})^n\\ - \frac{C^3}{6}(\phi_{i+1} - 3\phi_i + 3\phi_{i-1} - \phi_{i-2})^n\end{aligned} \tag{22}$$

where '$C$' is the Courent number ($\Delta t u/h$) with $h$ being the element size. The above equation leads to third-order time accurate scheme. It was proved in Reference [15] that this scheme is superior to the Taylor–Galerkin scheme. Although the above method avoids complexity introduced by the direct methods to some extent, the calculation of the modified weighting function $W$ needs to be carried out. In the following section, we provide a simpler method, which essentially leads to the form similar to Equation (22).

### *4.3. A simple explicit Characteristic-based procedure*

Here we discuss a simple explicit Characteristic method, which we recommend for practical use. Our discussion on the Characteristic-Based Split (CBS) scheme in the following section, will be based upon this simple Characteristic method.

This method was first published in 1984 [10] and is fully described in numerous other publications. Its derivation involves a local Taylor expansion and we illustrate this in Figure 2. The scalar convection equation in one dimension along a characteristic becomes

$$\frac{\mathrm{d}\phi}{\mathrm{d}t}(x', t) = 0 \tag{23}$$

 

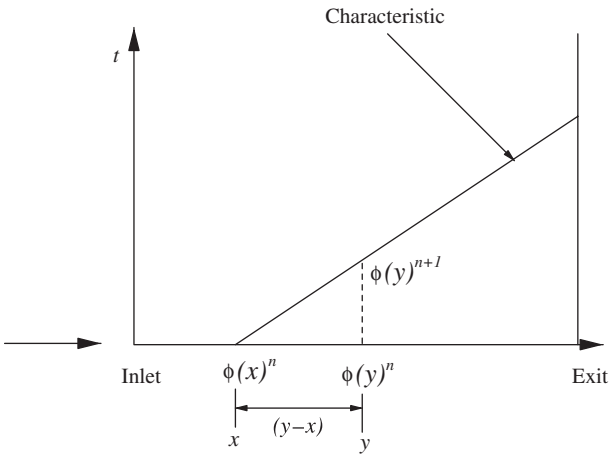


Figure 2. Linear convection problem. One Characteristic and the scalar variable at different levels.

where $x'$ represents the characteristic co-ordinates. The time discretization of the above equation leads to (see Figure 2)

$$\frac{\phi(y)^{n+1} - \phi(x)^n}{\Delta t} = 0 \tag{24}$$

If $\phi(y)^{n+1}$ can be analytically represented at $x$ the problem of projection can be avoided. Alternatively, $\phi(x)^n$ can be expressed in terms of $y$. Either way the complex integration methods used by the direct procedures can be avoided. The indirect method in the previous section explained one way of achieving this goal. However, we find it easier to use a Taylor expansion to determine a relation for $\phi(x)^n$ in terms of quantities at $y$. In order to proceed further we introduce the following Taylor expansion:

$$\phi^n(x) = \phi^n(y) - (y-x)\frac{\partial \phi(y)}{\partial x}^n + \frac{(y-x)^2}{2}\frac{\partial^2 \phi(y)}{\partial x^2}^n - \frac{(y-x)^3}{6}\frac{\partial^3 \phi(y)}{\partial x^3}^n + \cdots \tag{25}$$

In the above expansion, $(y-x)$ may be expressed in terms of time step and the average velocity within the characteristic segment as

$$y - x = \bar{u}\Delta t \tag{26}$$

Equation (25) now becomes

$$\phi^n(x) = \phi^n(y) - \Delta t\bar{u}\frac{\partial \phi(y)}{\partial x}^n + \frac{\Delta t^2\bar{u}^2}{2}\frac{\partial^2 \phi(y)}{\partial x^2}^n - \frac{\Delta t^3\bar{u}^3}{6}\frac{\partial^3 \phi(y)}{\partial x^3}^n + \cdots \tag{27}$$

Substitution of the above equation into Equation (24) leads to

$$\frac{\phi^{n+1}(y) - \phi^n(y)}{\Delta t} = -\bar{u}\frac{\partial \phi(y)}{\partial x}^n + \frac{\Delta t\bar{u}^2}{2}\frac{\partial^2 \phi(y)}{\partial x^2}^n - \frac{\Delta t^2\bar{u}^3}{6}\frac{\partial^3 \phi(y)}{\partial x^3}^n + O(\Delta t^3) \tag{28}$$

 

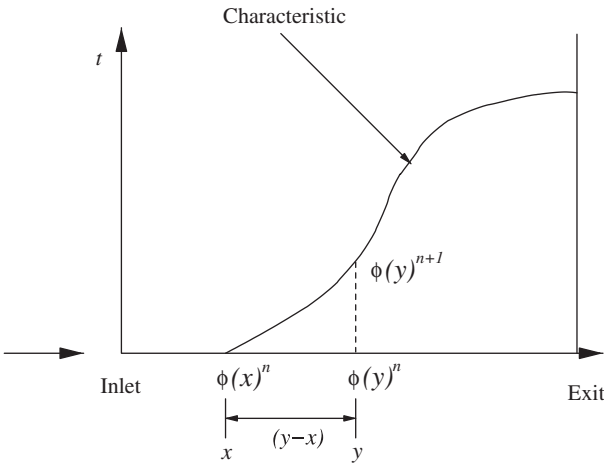


Figure 3. Non-linear convection problem. One Characteristic and the scalar variable at different levels.

For a linear convection equation the above equation is identical to Equation (22). It should also be noted that the average characteristic speed $\bar{u}$ is constant for a linear convection equation and no further approximation is necessary. However, for non-linear convection equation, further approximation is necessary. Equation (28) is non-conservation form of the convection equation and suitable for incompressible or divergence-free approximations with a constant speed. However, to derive conservation form of the equations with a non-linear propagation (see Figure 3) alternative approach is necessary. To derive a conservation form of the characteristic-based convection equation, we introduce an approximation for $u\phi(x)$ as

$$u\phi(x)^n = u\phi(y)^n - (y-x)\frac{\partial}{\partial x}(u\phi(y))^n + \frac{(y-x)^2}{2}\frac{\partial^2}{\partial x}(u\phi(y))^n - \frac{(y-x)^3}{6}\frac{\partial^3}{\partial x^3}(u\phi(y))^n \tag{29}$$

Assuming $\Delta t = (y-x)/u$ and substituting into Equation (24) we get

$$\frac{\phi(y)^{n+1}-\phi(y)^n}{\Delta t} = -\frac{\partial}{\partial x}(u\phi(y))^n + \frac{\Delta t}{2}u\frac{\partial^2}{\partial x^2}(u\phi(y))^n - \frac{\Delta t^2}{6}u^2\frac{\partial^3}{\partial x^3}(u\phi(y))^n + O(\Delta t^3) \tag{30}$$

which can be rewritten as

$$\frac{\phi(y)^{n+1}-\phi(y)^n}{\Delta t} = -\frac{\partial}{\partial x}(u\phi(y))^n + \frac{\Delta t}{2}u\frac{\partial}{\partial x}\left[\frac{\partial}{\partial x}(u\phi(y))\right]^n - \frac{\Delta t^2}{6}u^2\frac{\partial^2}{\partial x^2}\left[\frac{\partial}{\partial x}(u\phi(y))\right]^n + O(\Delta t^3) \tag{31}$$

 

The above equation is the conservation form of the simple explicit characteristic-based method for a scalar convection equation. The above equation will form the basis of our discretization procedure of fluid dynamics equations in the next section.

*Remark 1*
When dealing with a scalar convection problem, the variable convected becomes a characteristic variable and the speed at which it is convected becomes the characteristic speed. However, such an observation is not directly extended to a set of coupled conservation equations.

*Remark 2*
Although Equation (31) is third-order time accurate, it is seldom possible to achieve such higher order accuracy using linear finite elements as establishing the third-order spatial derivatives is difficult here. The multi-step strategies, such as the one employed by Taylor–Galerkin methods, could be employed for evaluating higher order derivatives but present study is limited to second-order derivatives.

For a convection–diffusion problem the simple characteristic-based procedure takes the following form without higher order terms:

$$\frac{\phi(y)^{n+1}-\phi(y)^n}{\Delta t} = -\frac{\partial}{\partial x}(u\phi(y))^n + \frac{\partial}{\partial x}\left(k\frac{\partial \phi}{\partial x}(y)\right)^n + \frac{\Delta t}{2}u\frac{\partial}{\partial x}\left[\frac{\partial}{\partial x}(u\phi(y)) - \frac{\partial}{\partial x}\left(k\frac{\partial \phi}{\partial x}(y)\right)\right]^n + O(\Delta t^2) \tag{32}$$

The third-order terms in the above equation could be neglected for linear elements. However, for higher order elements this term needs to be included.

## 5. CHARACTERISTIC-BASED SPLIT (CBS) SCHEME

Here both explicit and semi-implicit form of the CBS procedure are described. The fully explicit forms need no solution of simultaneous system of equations but the semi-implicit form needs implicit solution to the pressure Poisson equation. In practice we find the fully explicit form much easier to handle. We now describe the Characteristic-Based-Split (CBS) algorithm.

For the solution of the Navier–Stokes equations, the CBS algorithm uses a fractional step with a split. The four steps can be briefly described as (following Equation (32))

1. solve momentum equation without pressure terms,
2. calculate pressure from a Poisson equation,
3. correct the velocities, and finally
4. calculate any additional scalar variables such as temperature, concentration, etc. from appropriate governing equations.

 

In the first step, we define a new variable $U_i^*$ such that

$$U_i^* - U_i^n = \Delta t \left[ -\frac{\partial}{\partial x_j}(U_i u_j) + \frac{\partial \tau_{ij}}{\partial x_j} - \rho g_i \right]^n + \frac{\Delta t^2}{2} u_k \frac{\partial}{\partial x_k} \left( \frac{\partial}{\partial x_j}(U_i u_j) - \frac{\partial \tau_{ij}}{\partial x_j} + \rho g_i \right)^n \tag{33}$$

This represents the first part of the split and is explicit. The corrected velocities can be determined, once the pressure is known, using the equation

$$U_i^{n+1} - U_i^* = -\Delta t \frac{\partial p^{n+\theta_2}}{\partial x_i} + \frac{\Delta t^2}{2} u_k \frac{\partial}{\partial x_k} \left( \frac{\partial p^n}{\partial x_i} \right) \tag{34}$$

where $0 \leqslant \theta_2 \leqslant 1$ ($\theta_2 = 0$ for fully explicit scheme and $\theta_2 > 0$ for semi-implicit scheme).

The solution of this equation is actually the third step in the algorithm. The second step is the determination of the pressure. Referring to Equation (5), we can write

$$\left( \frac{1}{c^2} \right)^n (p^{n+1} - p^n) = -\Delta t \frac{\partial U_i^{n+\theta_1}}{\partial x_i} \tag{35}$$

Now $U_i^{n+\theta_1} \equiv \theta_1 U_i^{n+1} + (1 - \theta_1) U_i^n$ where $0.5 \leqslant \theta_1 \leqslant 1$, and using Equation (34) we get

$$U_i^{n+\theta_1} = \theta_1 \left[ U_i^* - \Delta t \frac{\partial p^{n+\theta_2}}{\partial x_i} + \frac{\Delta t^2}{2} u_k \frac{\partial}{\partial x_k} \left( \frac{\partial p^n}{\partial x_i} \right) \right] + (1 - \theta_1) U_i^n \tag{36}$$

and hence Equation (35) becomes

$$\left( \frac{1}{c^2} \right)^n (p^{n+1} - p^n) = -\Delta t \left[ \theta_1 \frac{\partial U_i^*}{\partial x_i} + (1 - \theta_1) \frac{\partial U_i^n}{\partial x_i} \right] + \Delta t^2 \theta_1 \frac{\partial}{\partial x_i} \left[ \theta_2 \frac{\partial p^{n+1}}{\partial x_i} + (1 - \theta_2) \frac{\partial p^n}{\partial x_i} - \frac{\Delta t}{2} u_k \frac{\partial}{\partial x_k} \left( \frac{\partial p^n}{\partial x_i} \right) \right] \tag{37}$$

The three step solution procedure may be summarized as (i) Calculating intermediate momentum field from Equation (33) (ii) Calculate pressure field from Equation (37) and (iii) Correct the momentum field using Equation (34). As a fourth step the energy equation is solved and the density is updated. The semi-discrete characteristic form of energy equation is written as

$$\frac{(\rho E)^{n+1} - (\rho E)^n}{\Delta t} = -\frac{\partial}{\partial x_i}(u_i \rho E)^n + \frac{\partial}{\partial x_i} \left( k \frac{\partial T}{\partial x_i} \right)^n - \frac{\partial}{\partial x_i}(u_i p)^n + \frac{\partial}{\partial x_i}(\tau_{ij} u_j)^n - \rho g_i u_i^n + \frac{\Delta t}{2} u_k \frac{\partial}{\partial x_k} \left[ \frac{\partial}{\partial x_i}(u_i \rho E) - \frac{\partial}{\partial x_i} \left( k \frac{\partial T}{\partial x_i} \right)^n + \frac{\partial}{\partial x_i}(u_i p) - \frac{\partial}{\partial x_i}(\tau_{ij} u_j)^n + \rho g_i u_i \right]^n \tag{38}$$

 

The resulting equations are solved using a standard Galerkin finite element procedure. The computational domain is discretized into a mesh of non-overlapping finite elements. We employ only linear triangular or tetrahedron elements in this paper. The spatial discretization of the variables are carried out as

$$U_i = \sum_{a=1}^{m} N^a \overline{U}_i{}^a; \quad p = \sum_{a=1}^{m} N^a \overline{p}^a; \quad U_i^* = \sum_{a=1}^{m} N^a \overline{U}_i^{*a}; \quad \rho E = \sum_{a=1}^{m} N^a (\overline{\rho E})^a \tag{39}$$

where overline represents a nodal quantity, the superscript $a$ represents a node and $m$ is the number of nodes in an element.

The semi-discrete forms of the equations are now weighted by $\mathbf{N}^{\mathrm{T}}$ and integrated over the domain. In this paper we use only linear elements and the third and higher order terms are neglected in the following equations.

Employing Equation (39) into Equation (33) and integrating, the first step of the CBS scheme becomes

$$\mathbf{M}\Delta\bar{\mathbf{U}}_{\mathbf{i}}^* = \Delta t \left[-\mathbf{C}\bar{\mathbf{U}}_{\mathbf{i}} + \mathbf{K}_{\boldsymbol{\tau}_i} + \mathbf{F}_i\right] + \frac{\Delta t^2}{2}\left[\mathbf{K}_{\mathbf{u}}\bar{\mathbf{U}}_{\mathbf{i}} + \mathbf{F}_{\mathbf{u}_i}\right] + \mathbf{f}_{\boldsymbol{\tau}\mathbf{i}} \tag{40}$$

where

$$\mathbf{M} \equiv \int_\Omega \mathbf{N}^{\mathrm{T}}\mathbf{N}\,\mathrm{d}\Omega; \quad \mathbf{C} \equiv \int_\Omega \mathbf{N}^{\mathrm{T}} \frac{\partial}{\partial x_j}\mathbf{N}u_j\,\mathrm{d}\Omega; \quad \mathbf{F}_i \equiv \int_\Omega \mathbf{N}^{\mathrm{T}}\rho g_i\,\mathrm{d}\Omega$$

$$\mathbf{F}_{\mathbf{u}_i} \equiv \int_\Omega \mathbf{N}^{\mathrm{T}} u_k \frac{\partial}{\partial x_k}\rho g_i\,\mathrm{d}\Omega; \quad \mathbf{K}_{\mathbf{u}} \equiv \int_\Omega \mathbf{N}^{\mathrm{T}} u_k \frac{\partial}{\partial x_k}\left(\frac{\partial}{\partial x_j}\mathbf{N}u_j\right)\mathrm{d}\Omega$$

$$\mathbf{K}_{\boldsymbol{\tau}_i} \equiv \int_\Omega \mathbf{N}^{\mathrm{T}} \frac{\partial}{\partial x_j}\tau_{ij}\,\mathrm{d}\Omega; \quad \mathbf{f}_{\boldsymbol{\tau}_i} \equiv \int_\Gamma \mathbf{N}^{\mathrm{T}}\tau_{ij}n_j\,\mathrm{d}\Gamma$$

The final matrix form of second step becomes

$$(\tilde{\mathbf{M}} + \Delta t^2\theta_1\theta_2\mathbf{H})\Delta\bar{\mathbf{p}} = \Delta t[\mathbf{G}\bar{\mathbf{U}}_{\mathbf{i}}^n + \theta_1\mathbf{G}\Delta\bar{\mathbf{U}}_{\mathbf{i}}^* - \Delta t\theta_1\mathbf{H}\bar{\mathbf{p}}^n - \mathbf{f}_{\mathbf{p}}] \tag{41}$$

here

$$\tilde{\mathbf{M}} \equiv \int_\Omega \mathbf{N}^{\mathrm{T}}\frac{1}{c^2}\mathbf{N}\,\mathrm{d}\Omega; \quad \mathbf{G} \equiv \int_\Omega \frac{\partial \mathbf{N}^{\mathrm{T}}}{\partial x_i}\mathbf{N}\,\mathrm{d}\Omega$$

$$\mathbf{H} \equiv \int_\Omega \frac{\partial \mathbf{N}^{\mathrm{T}}}{\partial x_i}\frac{\partial \mathbf{N}}{\partial x_i}\,\mathrm{d}\Omega; \quad \mathbf{f}_{\mathbf{p}} \equiv \Delta t \int_\Gamma \mathbf{N}^{\mathrm{T}}\left[\bar{\mathbf{U}}_{\mathbf{i}}^n + \theta_1\left(\Delta\bar{\mathbf{U}}_{\mathbf{i}}^* - \Delta t\frac{\partial p}{\partial x_i}^{n+\theta_2}\right)\right] n_i^{\mathrm{T}}\,\mathrm{d}\Gamma$$

The final form of third step becomes

$$\Delta\bar{\mathbf{U}}_{\mathbf{i}} = \Delta\bar{\mathbf{U}}_{\mathbf{i}}^* + \mathbf{M}^{-1}\Delta t\left[\mathbf{G}(\bar{\mathbf{p}}^n + \theta_2\Delta\bar{\mathbf{p}}) - \frac{\Delta t}{2}\mathbf{P}\bar{\mathbf{p}}^n - \mathbf{f}_{\mathbf{c}}\right] \tag{42}$$

where

$$\mathbf{P} = \int_\Omega \frac{\partial}{\partial x_i}\mathbf{N}^{\mathrm{T}}u_i\frac{\partial \mathbf{N}}{\partial x_j}\,\mathrm{d}\Omega; \quad \mathbf{f}_{\mathbf{c}} = \int_\Gamma (p + \theta_2\Delta p)n_i\,\mathrm{d}\Gamma \tag{43}$$

 

Finally, the energy equation can be written in the following form:

$$\mathbf{M}\Delta\bar{\mathbf{E}} = -\Delta t\left[\mathbf{C}_E\bar{\mathbf{E}} + \mathbf{C}_{\mathbf{p}}\bar{\mathbf{p}} + \mathbf{K}_T\bar{\mathbf{T}} + \mathbf{K}_{\tau E}\bar{\mathbf{u}} + \mathbf{f}_E - \frac{\Delta t}{2}(\mathbf{K}_{uE}\bar{\mathbf{E}} + \mathbf{K}_{up}\bar{\mathbf{u}})\right]^n \tag{44}$$

here $\bar{\mathbf{E}}$ is the nodal value of $\rho E$ and

$$\mathbf{C}_E \equiv \mathbf{C}_{\mathbf{p}} \equiv \mathbf{C}; \quad \mathbf{K}_T \equiv k\mathbf{H}; \quad \mathbf{K}_{\tau E} \equiv \mathbf{K}_\tau; \quad \mathbf{K}_{uE} \equiv \mathbf{K}_{up} \equiv \mathbf{K}_u$$

$$\mathbf{f}_E \equiv \int_\Gamma \mathbf{N}^{\mathrm{T}}\left(\tau_{ij}u_i + k\frac{\partial T}{\partial x_i}\right)n_i\,\mathrm{d}\Gamma$$

In the above equations $\Omega$ represents the entire computational domain and $\Gamma$ represents the boundaries. It is important to remark here that although equal order interpolation for all variables are assumed in the above equations, different order interpolations are certainly possible.

### *5.1. Boundary conditions*

The prescription of boundary conditions is discussed in many of our earlier publications [23, 31]. Here, we briefly discuss the Neumann boundary conditions. The boundary traction may be written as

$$t_i = \tau_{ij}n_j - pn_i \tag{45}$$

Due to the removal of pressure term from the first step, only part of the traction (deviatoric part) appears in step one and pressure part appears at the third step. However, it is now accepted that the total traction can be prescribed at the first step and no traction is needed at the third step.

The second step contains the following boundary term:

$$\begin{aligned}\int_\Gamma \mathbf{N}^{\mathrm{T}}\left[\bar{\mathbf{U}}_{\mathbf{i}}^n + \theta_1\left(\Delta\bar{\mathbf{U}}_{\mathbf{i}}^* - \Delta t\frac{\partial p}{\partial x_i}^{n+\theta_2}\right)\right]n_i^{\mathrm{T}}\,\mathrm{d}\Gamma \\ \approx \int_\Gamma \mathbf{N}^{\mathrm{T}}\left[\bar{\mathbf{U}}_{\mathbf{i}}^n + \theta_1\Delta\mathbf{U}_i\right]n_i^{\mathrm{T}}\,\mathrm{d}\Gamma \\ = \int_\Gamma \mathbf{N}^{\mathrm{T}}\left[\mathbf{U}_i\right]n_i^{\mathrm{T}}\,\mathrm{d}\Gamma\end{aligned} \tag{46}$$

On the solid walls the above quantity is equal to zero. Rest of the Neumann boundary conditions are standard and straight forward to implement. The boundary terms resulting from the convection stabilizing terms are not included as the residual of the governing equation is expected to vanish on the boundaries.

*Remark 3*

The above steps introduces second-order convection stabilizing terms mainly in steps one and four (energy equation). These terms are functions of time step. Unlike other stabilizing

 

algorithms the optimal value of the stabilizing parameter is chosen to be $\Delta t/2$. However, equivalent parameters as a function of element size in the stream line direction is not ruled out [48].

*Remark 4*
Pressure stabilization is introduced via the second-order pressure terms in the second step. Again the time step is part of the stabilization process. These terms indicate that the time step values should lie as close to stability limit as possible. Too small time step values can lead to spurious pressure oscillations [44].

## 6. TREATMENT OF COMPRESSIBLE FLOW PROBLEMS

Three further steps are necessary to get a smooth solution at all Mach numbers. They are additional artificial viscosity for shock capturing, solution smoothing at very low Mach numbers and temperature dependent viscosity calculation. In this section we provide a brief summary of these additional treatments

### *6.1. Artificial dissipation*

At transonic and supersonic speeds, an additional shock capturing dissipation is necessary to capture shocks and to smooth local oscillations in the vicinity of shocks. There are several potential shock capturing techniques possible for treating the shocks. We have been employing the second derivative-based methods with success for treating shocks. We found the pressure switch-based methods efficient for inviscid flow problems and the second derivative-based methods without any approximation suitable for viscous flow problems.

A recommended shock capturing viscosity method for compressible inviscid flow problems, given by Nithiarasu *et al.* [26] and Morgan *et al.* [47] is adopted here. For a scaler field variable $\phi$ the smoothed values, $\phi_s$ are computed by

$$\left[\frac{\overline{\boldsymbol{\phi}}_s^{n+1}-\overline{\boldsymbol{\phi}}^{n+1}}{\Delta t}\right]=\mathbf{M_L^{-1}}\frac{C_e S_e}{\Delta t_e}\left(\mathbf{M}-\mathbf{M_L}\right)\overline{\boldsymbol{\phi}}^n \tag{47}$$

Here $S_e$ is the element 'pressure switch' and is taken to be the mean of the element nodal switches $S_a$, which in turn are given by

$$S_a=\frac{|\Sigma_e(p_a-p_k)|}{\Sigma_e|p_i-p_k|} \tag{48}$$

$C_e$ is an user specified constant ranging between 0.0 and 1.0 and $\Delta t_e$ is the local element time step. In Equation (48) the index $a$ denotes a node and $k$ denotes the nodes connected to $a$ [26, 47].

For viscous compressible flows we recommend the following form of shock capturing viscosity:

$$\left[\frac{\overline{\boldsymbol{\phi}}_s{}^{n+1}-\overline{\boldsymbol{\phi}}^{n+1}}{\Delta t}\right]=-\mathbf{M_L^{-1}}C_e h^3\,\frac{|\mathbf{u}|+c}{\bar{p}}\left|\frac{\partial^2 p}{\partial x_i^2}\right|_e^n\left(\int_\Omega \frac{\partial \mathbf{N}^{\mathrm{T}}}{\partial x_i}\,\frac{\partial \mathbf{N}}{\partial x_i}\,\mathrm{d}\Omega\right)\overline{\boldsymbol{\phi}}^n \tag{49}$$

 

where $h$ is the element size, $\bar{p}$ is an average element pressure and subscript $e$ represents an element.

One of the artificial dissipation schemes discussed above is added to the discrete form of first, second and fourth steps of the CBS scheme when a transonic or supersonic problem is solved.

### 6.2. Variable smoothing at low Mach numbers

In order to compute very low Mach number flows, a variable smoothing procedure is adopted in the place of artificial shock capturing diffusion. The following equation defines the variable smoothing applied to the transport variables, $\{\mathbf{\Phi}\}$:

$$\{\mathbf{\Phi}\} = \left[\frac{1}{1+0.5\alpha}\{\mathbf{\Phi}\} + \frac{\alpha}{1+0.5\alpha}[\mathbf{M} - \mathbf{M_D}]\mathbf{M_L^{-1}}\{\mathbf{\Phi}\}\right] \tag{50}$$

where $\alpha$ is a variable smoothing parameter varies between 0 and 0.05, $\mathbf{M}$ is the consistent mass matrix, $\mathbf{M_D}$ is the consistent mass matrix without non-diagonal terms and $\mathbf{M_L}$ is the lumped mass matrix. By increasing $\alpha$ the weighting on the node in question is decreased while the influence of the surrounding nodes is increased [48].

### 6.3. Sutherland's relation for temperature dependent viscosity

The Sutherland's temperature dependent viscosity relation may be written in SI system of units for air as [49]

$$\mu = \frac{1.45T^{3/2}}{T+110} \times 10^{-6} \tag{51}$$

where $T$ is in Kelvin.

## 7. TREATMENT OF INCOMPRESSIBLE FLOW EQUATIONS

Incompressible flows need no special treatment if the semi-implicit form of the solution procedure is used. However, if the fully explicit form of the solution is desired then it is essential to introduce the artificial compressible wave speed into the continuity equation as

$$\frac{1}{\beta^2}\frac{\partial p}{\partial t} + \rho\frac{\partial u_i}{\partial x_i} = 0 \tag{52}$$

This way one can treat the continuity equation explicitly to reach a steady state solution. Here, $\beta$, the artificial compressibility parameter is finite instead of infinity in purely incompressible flows. However, $\beta$ will have no influence on the steady state solution. The recommended $\beta$ value is calculated as

$$\beta = \max\left(\varepsilon, \sqrt{u_i u_i}, \frac{2v}{h}\right) \tag{53}$$

 

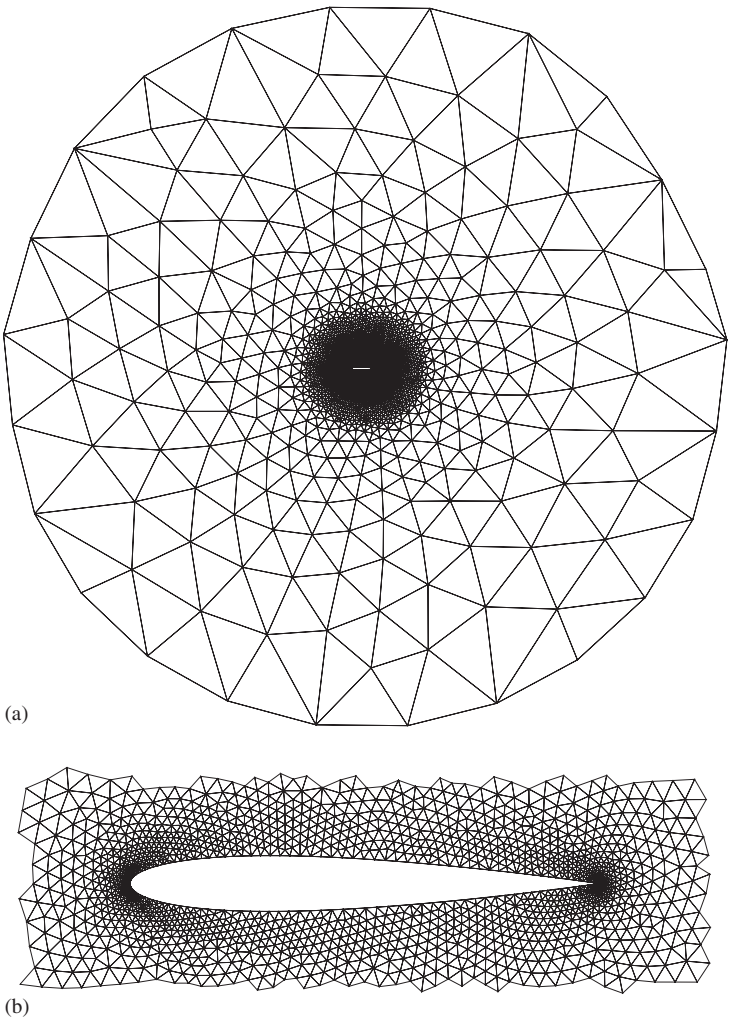


Figure 4. Inviscid flow past a NACA0012 aerofoil. Unstructured mesh. Number of nodes: 3753; number of elements: 7351: (a) finite element mesh and domain; and (b) mesh distribution in the vicinity of the aerofoil.

where $\varepsilon$ is a small real number. The optimal value (from experience) of this quantity is 0.5. Another issue to be addressed here is how to recover the real time solution. The answer is in the use of dual time stepping method. In a dual time stepping method additional real time terms are added to the momentum equation. When using the CBS scheme this is added to the third step of the scheme. The calculation goes through an iterative process in which two loops are employed. Within the inner loop the variables $u_i$ and $p$ are converged to a local steady state using local time steps and then in the outer loop the calculation enters the next real time step.

 

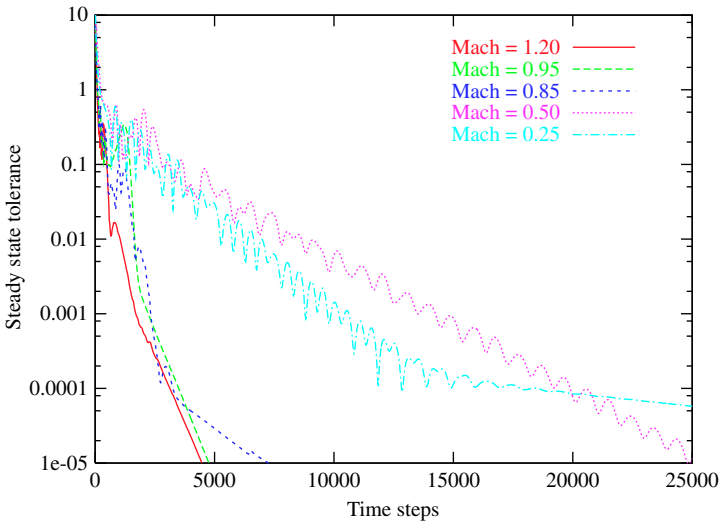


Figure 5. Inviscid flow past a NACA0012 aerofoil. Convergence histories to steady state.

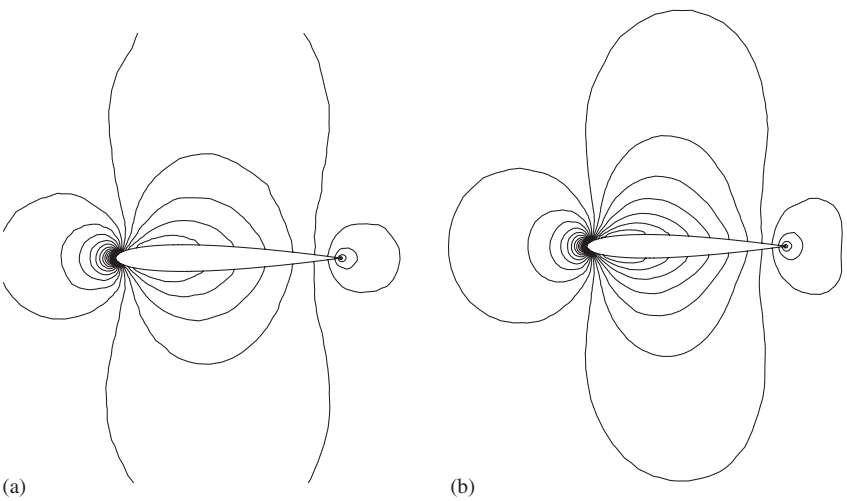


Figure 6. Inviscid subsonic flow past NACA0012 aerofoil. Pressure contours: (a) Mach number = 0.25; and (b) Mach number = 0.5.

## 8. LOCAL TIME STEPPING

Local time stepping is an important part of any explicit time stepping algorithm. In a local time stepping approach different time steps are used at different nodes and the solution is accelerated to steady state. Using globally minimum time step, the calculations to steady state takes much longer time than the local time stepping procedure. The following local time stepping approach

 

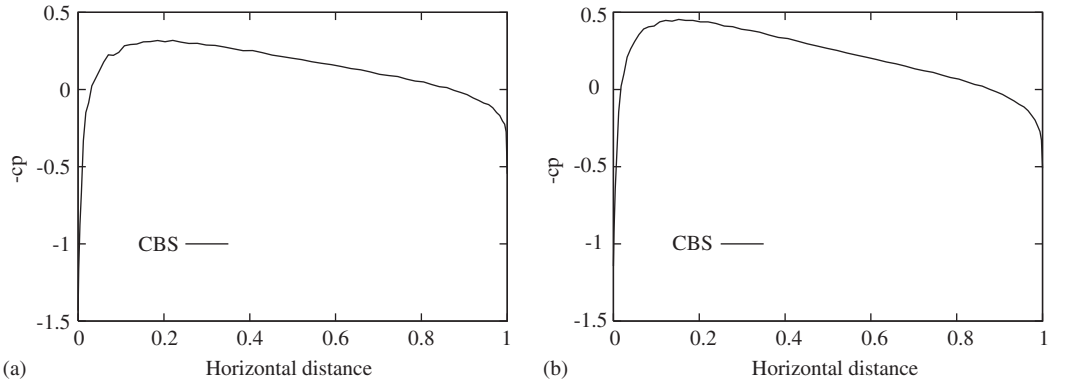


Figure 7. Inviscid subsonic flow past NACA0012 aerofoil. Pressure coefficient distribution: (a) Mach number = 0.25; and (b) Mach number = 0.5.

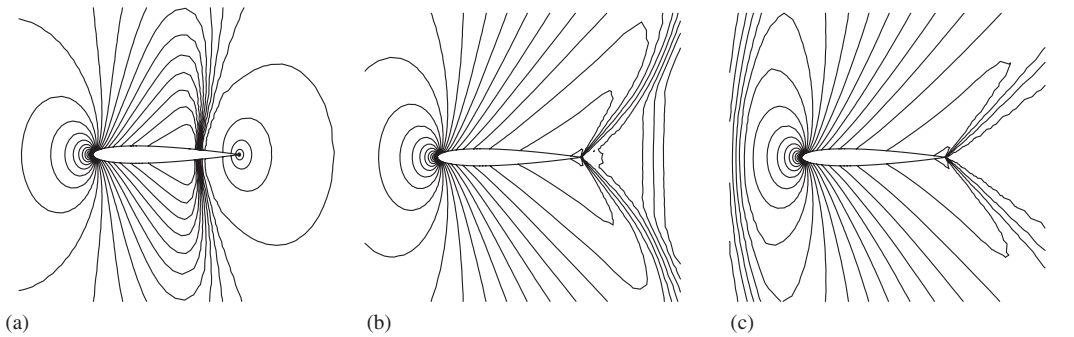


Figure 8. Inviscid transonic and supersonic flow past a NACA0012 aerofoil. Pressure contours: (a) Mach number = 0.85; (b) Mach number = 0.95; and (c) Mach number = 1.2.

is recommended:

$$\Delta t = \min(\Delta t_{\text{conv}}, \Delta t_{\text{diff}}) \tag{54}$$

where

$$\Delta t_{\text{conv}} = \frac{h}{|\mathbf{u}_{\text{conv}}| + c} \tag{55}$$

for compressible flows and

$$\Delta t_{\text{conv}} = \frac{h}{|\mathbf{u}_{\text{conv}}| + \beta} \tag{56}$$

for incompressible flows. The diffusion limit is given as

$$\Delta t_{\text{diff}} = \frac{h^2}{2\nu} \tag{57}$$

 

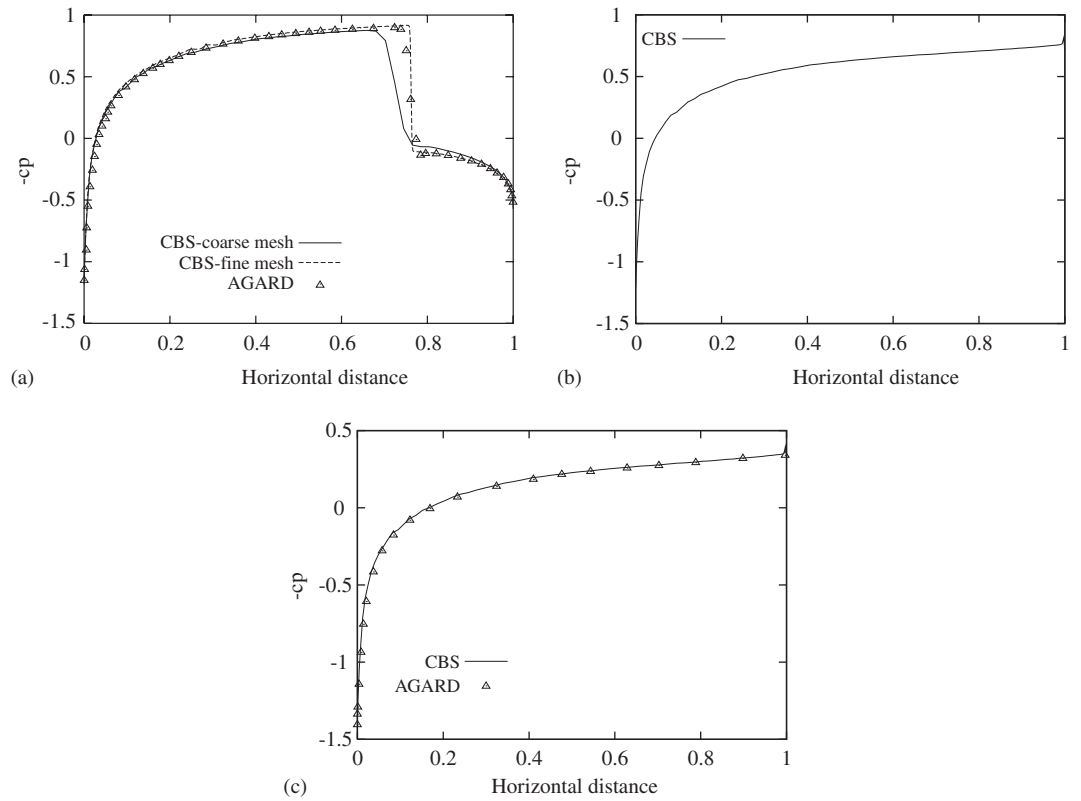


Figure 9. Inviscid transonic and supersonic flow past a NACA0012 aerofoil. Pressure Coefficient distribution: (a) Mach number = 0.85; (b) Mach number = 0.95; and (c) Mach number = 1.2.

The calculated $\Delta t$ is multiplied by a safety factor varying between 0.1 and 1.0 depending on the problem and mesh used. As mentioned before the time steps are calculated at nodes. It is therefore necessary to assign an appropriate element size, $h$, on the nodes. We recommend the following relations:

$$h_i = \min(3\text{Volume}/\text{Opposite face area})_{ie} \tag{58}$$

in three dimensional cases. In the above equation, minimum value is selected among the number of elements $ie$ connected to node $i$. Similarly

$$h_i = \min(2\text{Area}/\text{Opposite side length})_{ie} \tag{59}$$

in two dimensions. It is also possible to calculate the element sizes in the streamline direction to improve accuracy. However, the accuracy improvement has to be carried out at the expense of calculating time dependent element size [48].

 

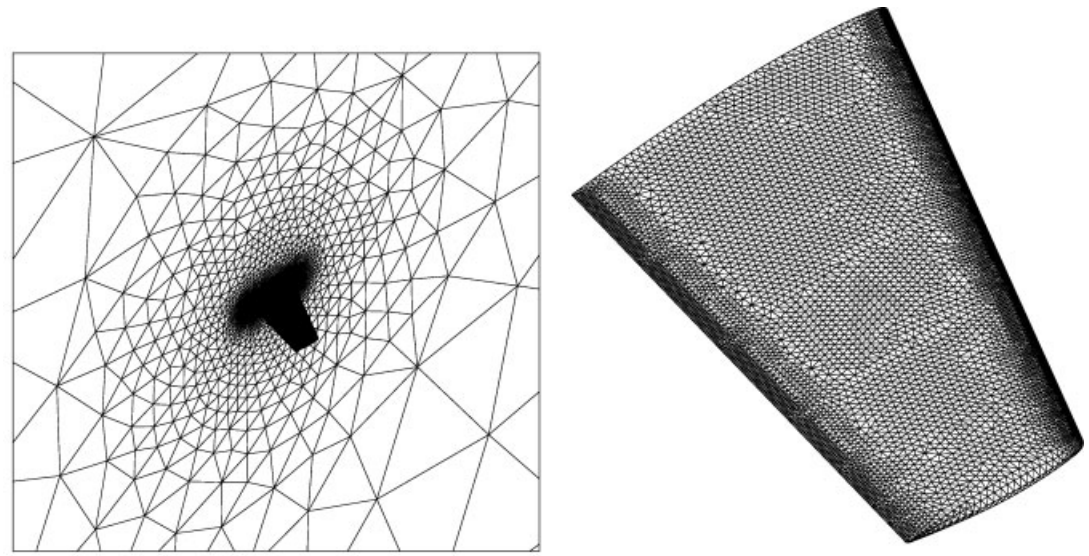


Figure 10. Inviscid flow past the ONERA M6 wing. Surface mesh. Number of nodes: 252 192; number of elements: 1 469 666: (a) surface mesh of the wing and vertical surface; and (b) surface mesh of the wing.

## 9. RESULTS AND DISCUSSION

All the problems presented in this paper are produced using a fully explicit form of solution procedure with lumped mass matrix. The simultaneous equations are not formed at any stage.

### *9.1. Compressible flows*

In this subsection some compressible inviscid and viscous problems are presented. The steady state tolerance is calculated as

$$e = \sqrt{\frac{\sum_{a=1}^{\text{nodes}} \left( \dfrac{\rho_a^{n+1} - \rho_a^n}{\Delta t} \right)^2}{\sum_{a=1}^{\text{nodes}} (\rho_a^{n+1})^2}} \tag{60}$$

The above equation is non-dimensionalized using a characteristic time scale of $(u_\infty/L)^{-1}$. The non-dimensional tolerance is reduced to at least $10^{-5}$ to obtain a steady state.

*9.1.1. Inviscid flow past a NACA0012 aerofoil.* The first problem considered is the inviscid flow past a NACA0012 aerofoil. Here we have solved this problem over a range of Mach numbers within subsonic, transonic and supersonic flow regimes at zero angle of attack. The problem domain and mesh used are shown in Figure 4. The diameter of the circular domain is equal to 25 times the chord length of the aerofoil. The leading edge of the aerofoil is assumed to be at the centre of the domain. All the inlet quantities are prescribed and no variable is

 

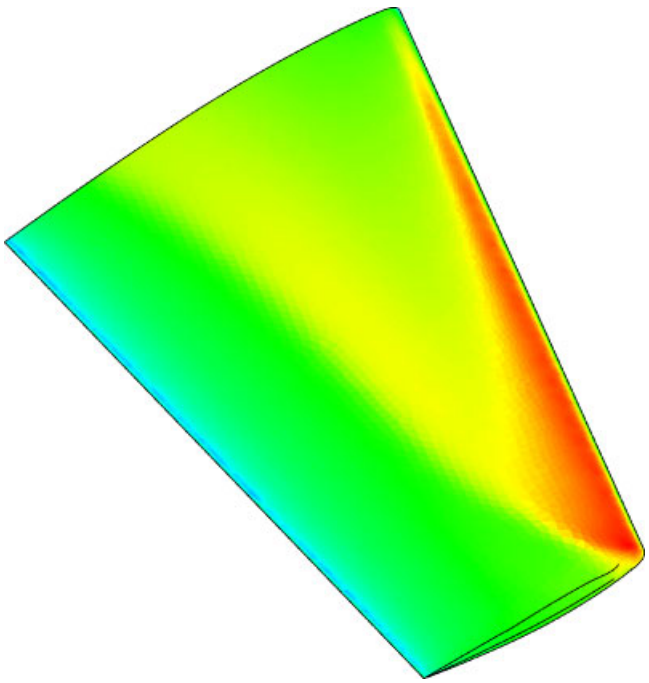

Figure 11. Inviscid flow past the ONERA M6 wing. Density contours.

prescribed at the exit at supersonic and transonic speeds. At subsonic speeds however, one of the primitive variables are prescribed at the exit. The Mach number is varied between 0.25 and 1.2 to capture all different flow regimes.

Figure 5 shows the steady state convergence histories at different Mach numbers. As expected convergence to steady state at supersonic and transonic Mach numbers is rapid but the subsonic cases took longer to reach steady state. The pressure coefficients are calculated as $-2(p_a - p_{\text{ref}})$. Here $p_{\text{ref}}$ is the reference pressure at inlet or exit.

Figures 6 and 7 show the pressure contours and surface pressure coefficient distribution at subsonic Mach numbers. At both subsonic Mach numbers, we invoke the variable smoothing in the place of shock capturing viscosities. A detailed comparison of stagnation quantities with analytical solution at subsonic Mach numbers is presented in Reference [48].

Figures 8 and 9 show the pressure contours and surface pressure coefficient distribution at transonic and supersonic Mach numbers. The qualitative agreement of the contours with standard benchmark results is excellent. In Figure 9 two pressure coefficient results are compared with the AGARD results. [50]. As seen the results are in good agreement with the AGARD results. In Figure 9(a), a mesh, finer than the one shown in Figure 4 was also used to prove that the convergence of the solution is achieved.

*9.1.2. Inviscid flow past the ONERA M6 wing.* The second inviscid flow problem studied is transonic flow past ONERA M6 wing at an angle of attack of 3°. The inlet Mach number is 0.8447. Figure 10 shows the surface mesh of the wing and the surface to which the wing

 

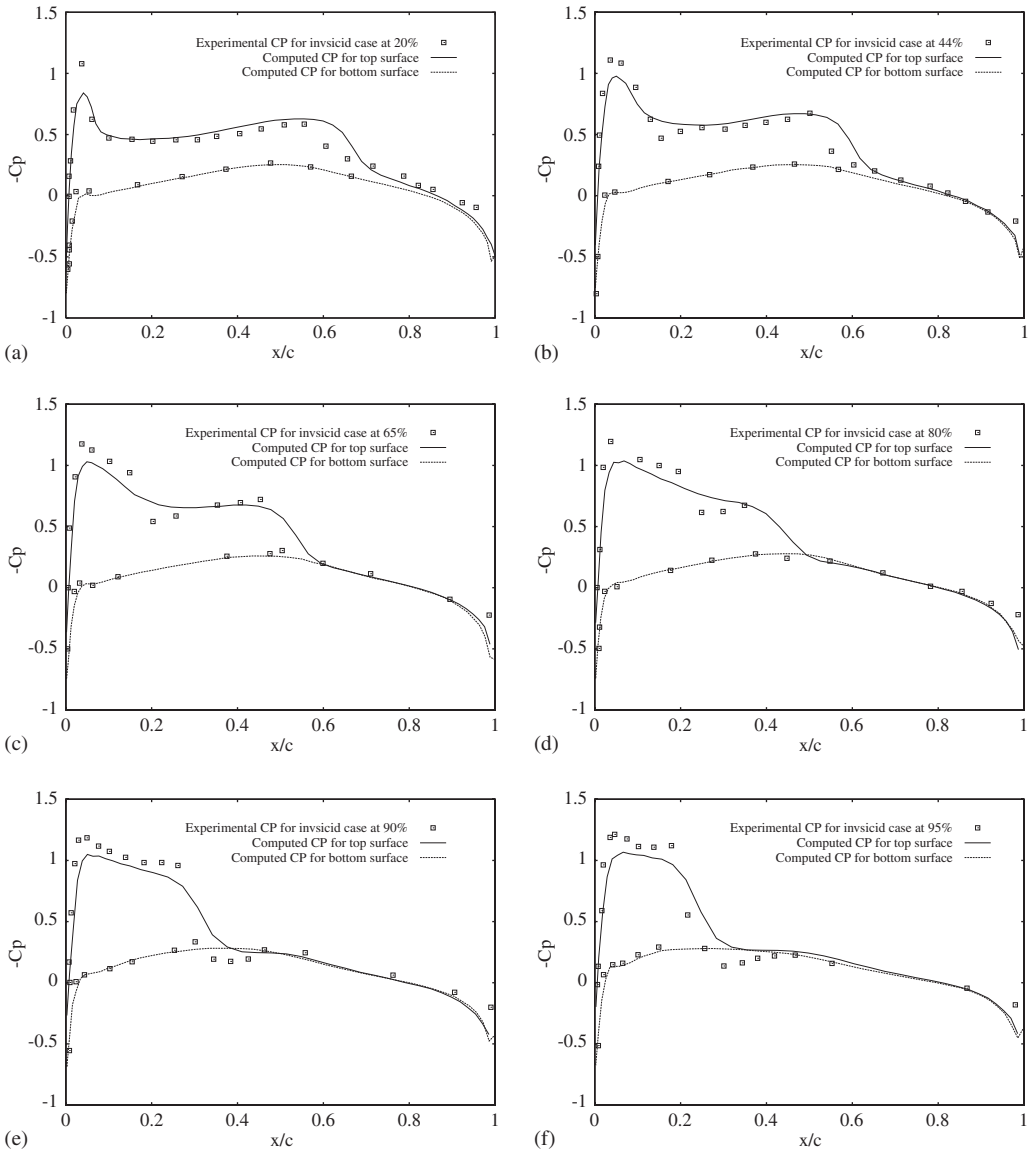


Figure 12. Inviscid flow past the ONERA M6 wing. Mach number = 0.85 and angle of attack 3°: (a) Mach number = 0.25; (b) Mach number = 0.5; (c) Mach number = 1.2; (d) Mach number = 0.25; (e) Mach number = 0.5; and (f) Mach number = 1.2.

is attached. A far stream semi-circular boundary is created with a diameter equal to 26 times the base chord length of the wing. This problem has been widely studied as a benchmark case for testing 3D compressible flow codes. Experimental pressure coefficients are available to compare the predicted results. The boundary conditions are similar to the previous two-dimensional problem. All variables except pressure and density are prescribed at the inlet.

 

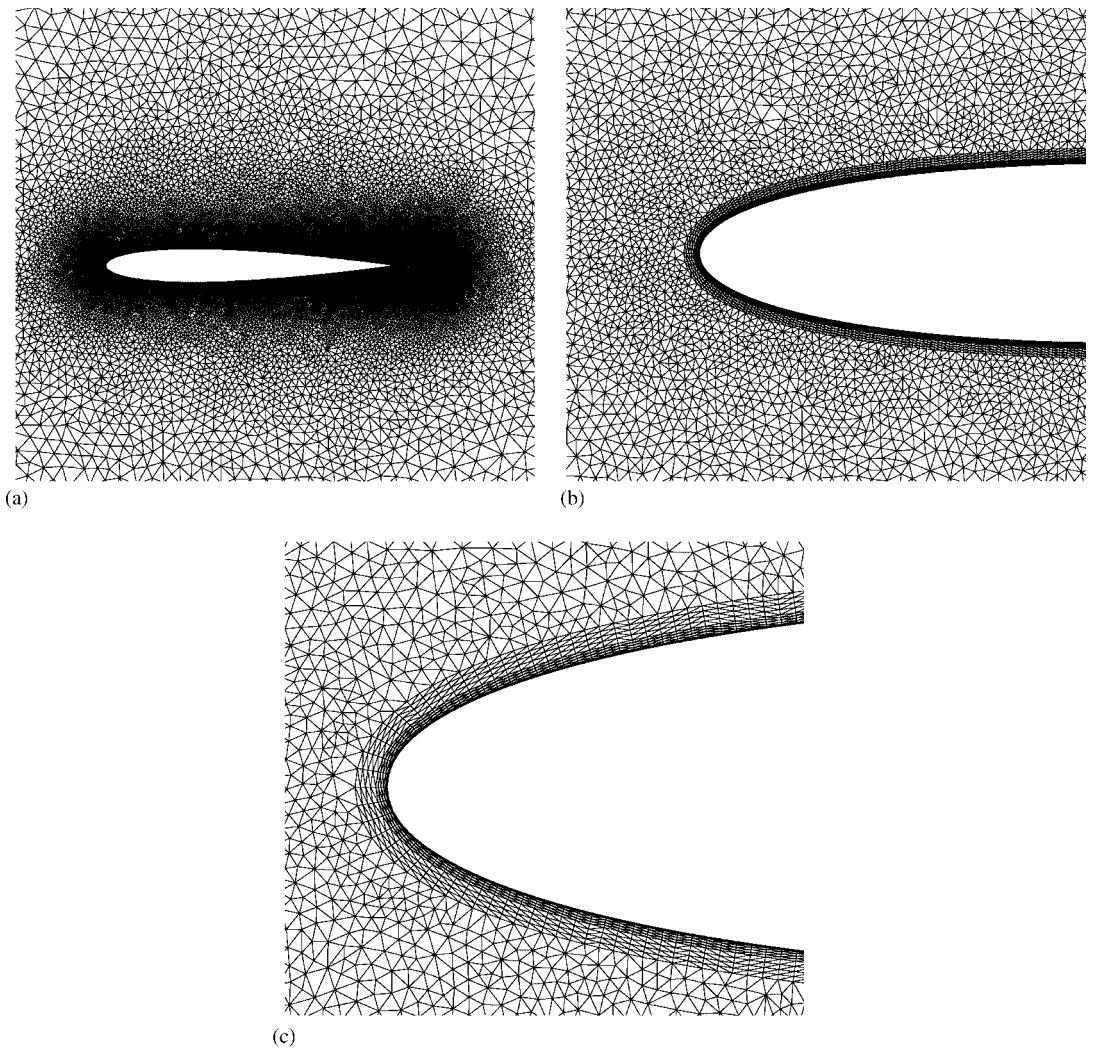


Figure 13. Finite element mesh. Number of nodes: 8425; number of elements: 16 496: (a) finite element mesh in the vicinity of the aerofoil; (b) structured layers close to the aerofoil surface; and (c) close-up view of structured layers.

Figure 11 shows the surface density contours on the top surface of the wing. As seen the shock waves on the surface display the qualitative behaviour similar to the ones reported by others. In Figure 12 we compare pressure coefficient at various sections of the wing. As seen the agreement between the calculations and experimental data is generally good.

*9.1.3. Transonic viscous flow past a NACA0012 aerofoil.* The first viscous compressible flow problem considered here is that of transonic flow past a NACA0012 aerofoil with zero angle of attack at a moderate Reynolds number of 2000 and at an inlet Mach number of 0.85.

 

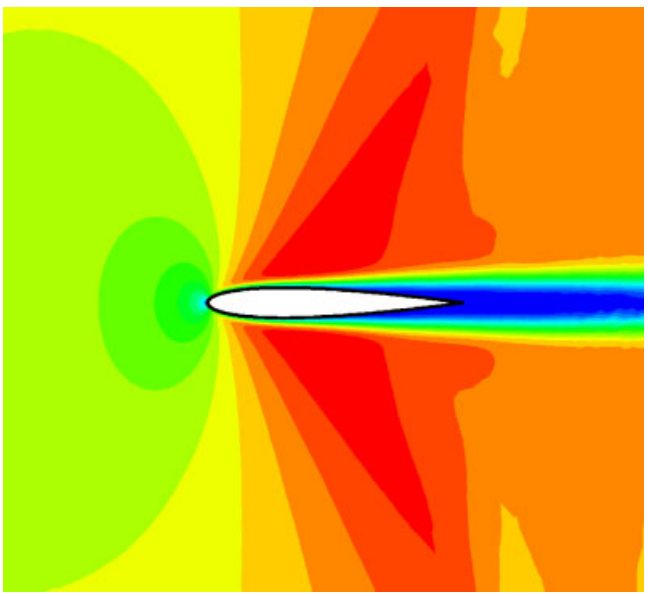

Figure 14. Mach contours.

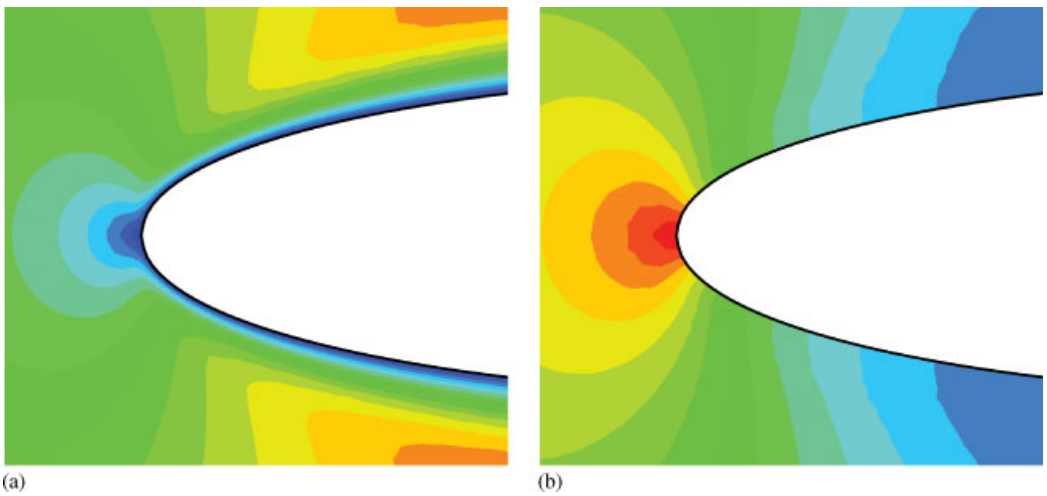


Figure 15. Mach and pressure contours: (a) Mach contours in the vicinity of stagnation point; and (b) pressure contours in the vicinity of the stagnation point.

In Figure 13 we show the mesh used for this purpose. The mesh is fine and structured close to the aerofoil surface and highly unstructured away from the wall. This type of hybrid meshes are generated by growing normals from the aerofoil surface. For further details on this type of mesh generation, readers are referred to relevant publications [51–56].

 

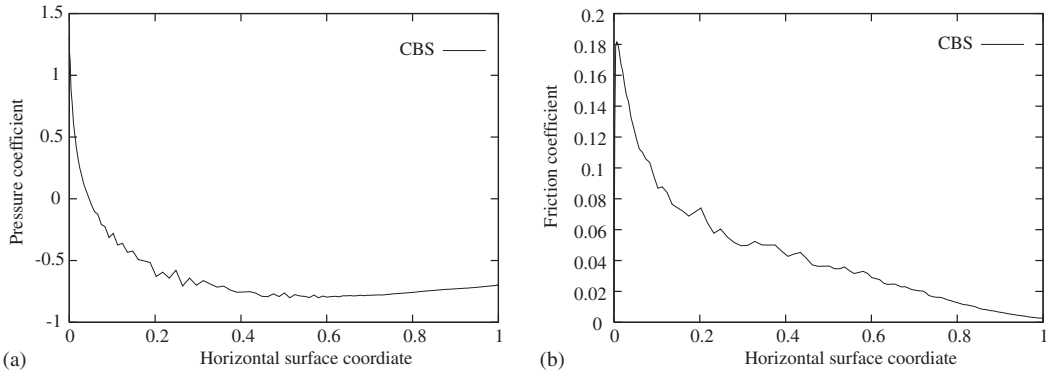


Figure 16. Pressure and friction coefficient distribution: (a) pressure coefficient; and (b) friction coefficient.

The external domain size used is circular with a diameter equal to 25 times the chord length. In addition to usual far field boundary conditions, no-slip boundary conditions are prescribed on the walls of the aerofoil. The temperature dependent viscosity is computed using Sutherland's empirical relation given by Equation (51).

Figures 14 and 15 show the contours of Mach number and pressure. The contours are in good agreement with the reported fully structured mesh solution [57, 58]. Figure 15 also emphasize the point that the inherent stabilization mechanism of CBS procedure gives smooth solution in the vicinity of stagnation points.

Figure 16 gives the pressure coefficient and skin friction coefficient distribution along the chord of the aerofoil.

*9.1.4. Hypersonic viscous flow past a double ellipsoid.* The second viscous compressible flow problem considered is hypersonic flow past a double ellipsoid. The mesh used is structured close to the wall and unstructured away from the wall as shown in Figure 17. The mesh used is adapted to capture the bow shock. More details on the mesh adaption is available in other relevant publications. In Figure 18 we show the density contours and the strong bow shock in front of the ellipsoid. A free stream Mach number of 8.125 and a Reynolds number of 100 000 along with an angle of attack of 30° were used here [51].

### *9.2. Incompressible flow problems*

In this subsection two incompressible flow problems are solved using purely unstructured meshes. The convergence to steady state is determined by the criterion given by Equation (60) but the density in this relation is replaced with velocity here.

*9.2.1. Laminar flow past a sphere.* The first incompressible flow problem considered is the laminar flow past a single sphere placed inside an imaginary box as shown in Figure 19. The computational domain is a rectangular box of length $25D$, where $D$ is the diameter of the sphere, with the downstream boundary located $20D$ from the centre of the sphere. The four side walls are located at a distance of $5D$ from the centre of the sphere. All four confinement

 

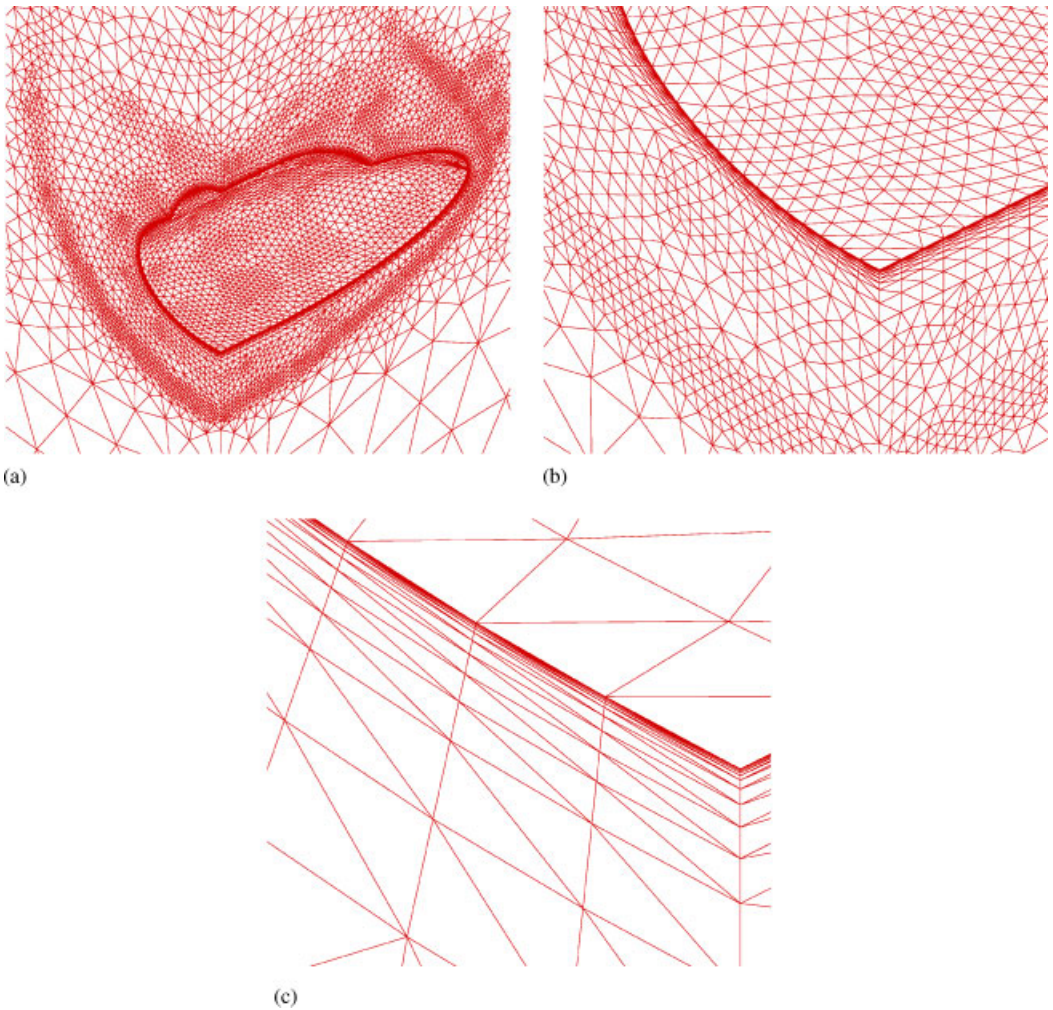


Figure 17. Finite element meshes: ((a), (b) and (c)). Number of node: 79 023; number of elements: 441 760.

walls are assumed to be slip walls with normal velocity equal to zero. The inlet velocity is assumed to be uniform and the no-slip condition prevails on the sphere surface.

For this, an unstructured grid containing 953 025 tetrahedral elements was used. Figure 20 shows the contours of the $u_1$ component of the velocity and pressure contours at Reynolds numbers of 100 and 200. Figure 21 compares the $c_p$ values on the surface along the flow axis with those available in literature.

Note that the results used for comparison were generated using very fine structured meshes [59, 60]. It should also be noted that all the results differ from each other close to separation zone.

 

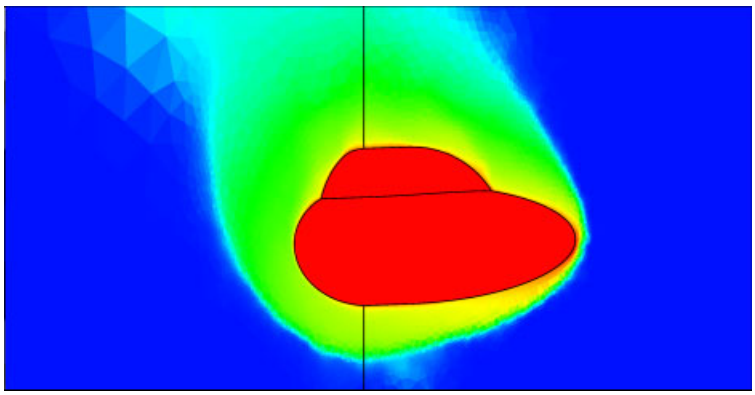

Figure 18. Mach contours.

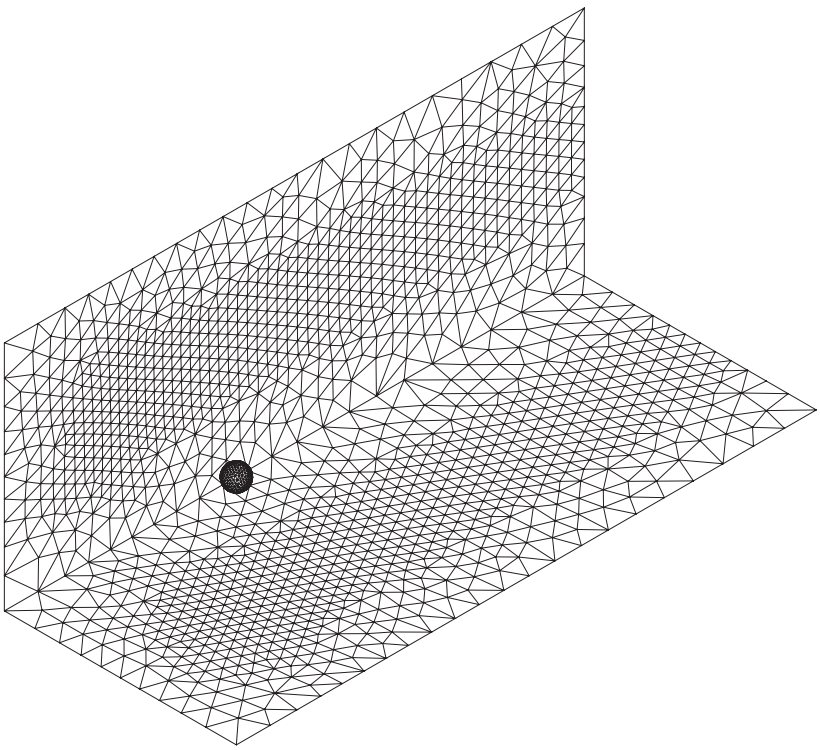

Figure 19. Laminar steady flow past a sphere. Surface mesh. Total number of nodes in the volume mesh: 164 139; number of elements: 953 025.

*9.2.2. Laminar flow within a model human upper airway.* Here, flow through a model human upper airway is investigated. The geometry used is generated from the data provided in Reference [61] along with the model given in Reference [62]. The model represents the airflow

 

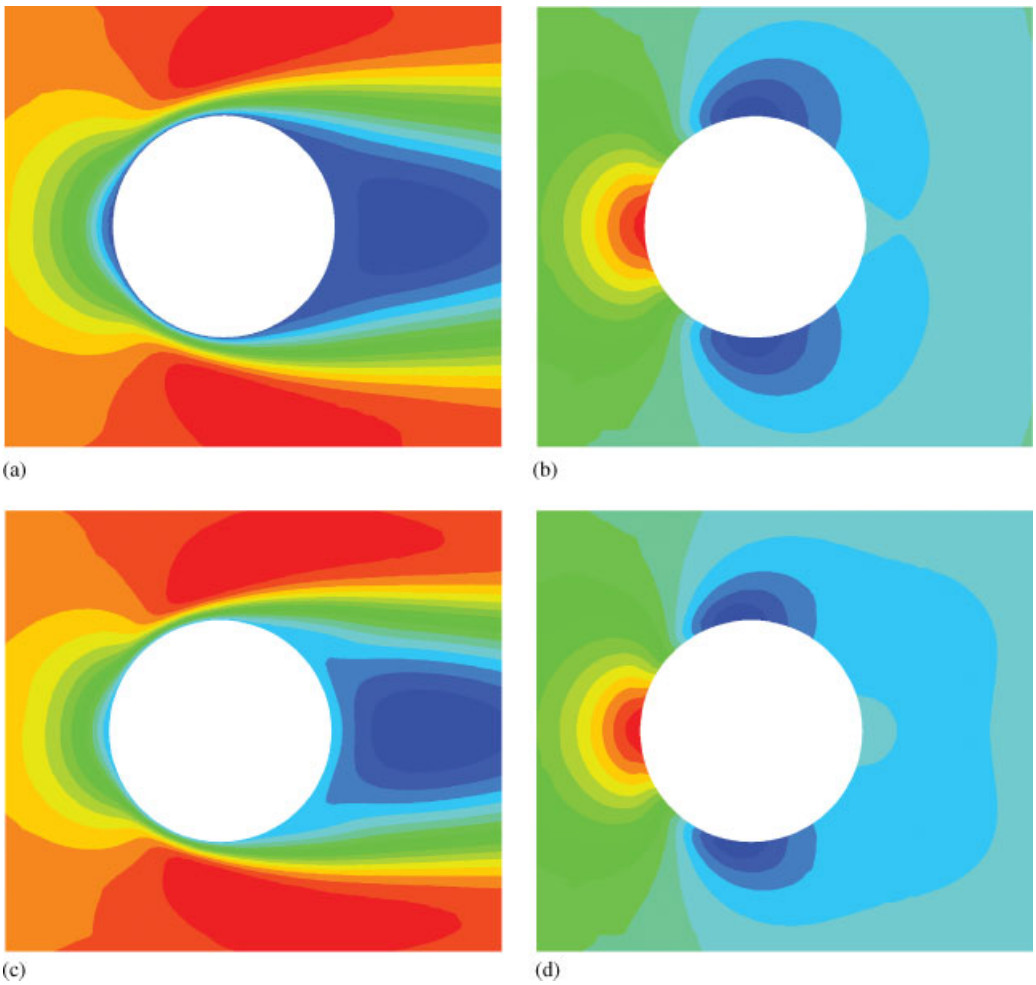


Figure 20. Laminar steady flow past a sphere. $u_1$ and pressure contours: (a) $u_1$ velocity contours, $Re = 100$; (b) pressure contours, $Re = 100$; (c) $u_1$ velocity contours, $Re = 200$; and (d) pressure contours, $Re = 200$.

from mouth to trachea. It should be noted that there are other studies available on particle movement in the upper human airways using either structured or semi-structured meshes [63–65]. Fluid dynamics analysis of such a problem can help understand many problems associated with the human airways such as 'Sleep Apnoea', airway obstructions, vocal-cord related problems and spray dynamics.

The mesh used in the present study is shown in Figure 22. This mesh contains just over two million unstructured tetrahedral elements. The walls of the upper airway is assumed to be rigid and the flow is assumed to be from mouth (left) to the trachea (right). The flow is assumed to enter the mouth at a uniform constant velocity in the normal direction. The Reynolds number

 

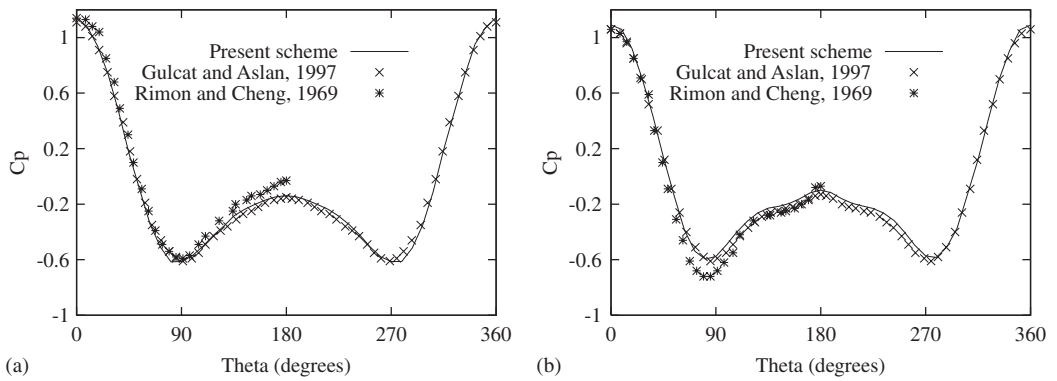


Figure 21. Laminar steady flow past a sphere. Pressure coefficient distribution: (a) $Re = 100$; and (b) $Re = 200$.

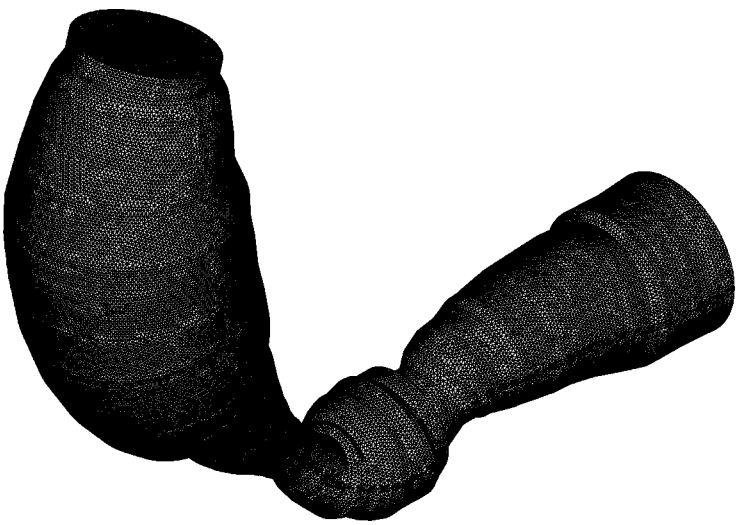

Figure 22. Flow through a model human upper airway. Unstructured surface mesh.

is defined based on the size of the smallest section (epiglottis) and inlet velocity. Usual no-slip boundary conditions are assumed on the walls and at exit zero pressure values are used. No pressure values are prescribed at the inlet.

Figure 23 shows the cross-sectional view along the length of the airway. This figure shows the contours of all velocity components and pressure at a Reynolds number of 10. The contours are generally smooth. In Figure 24 we also show the surface pressure distribution near the narrow portion (epiglottis). As expected the pressure gradient is very high close to this narrow portion.

 

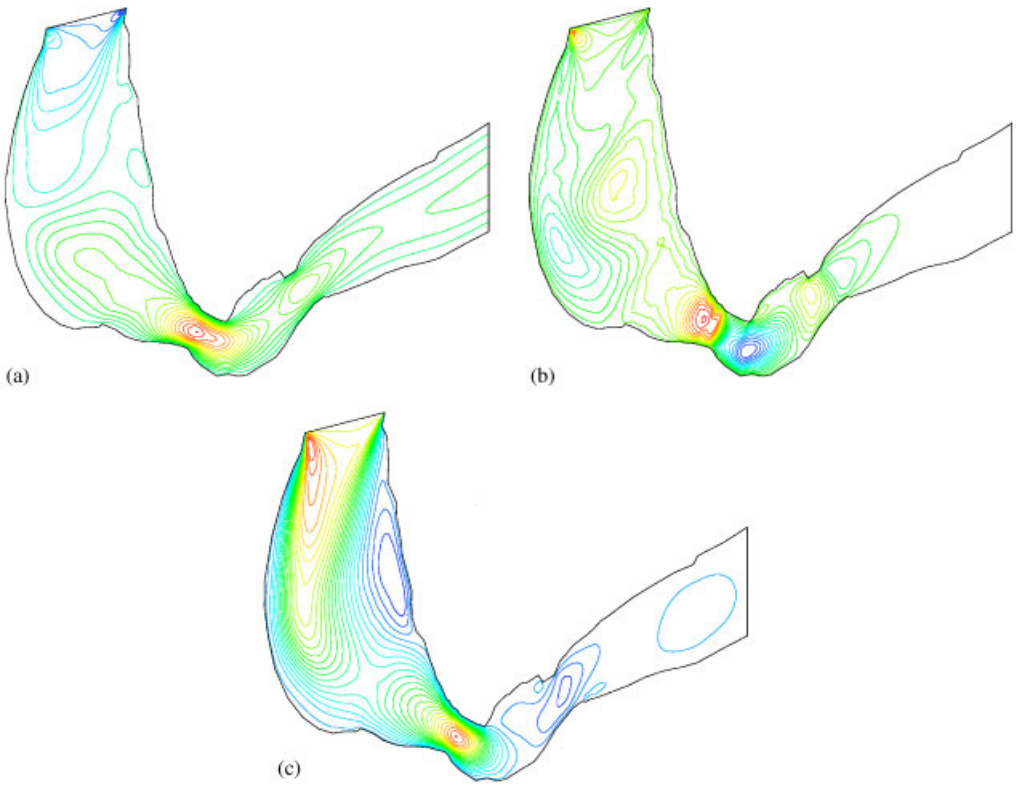


Figure 23. Flow through a model human upper airway. Cross-sectional view: (a) $u_1$ velocity contours; (b) $u_2$ velocity contours; and (c) $u_3$ velocity contours.

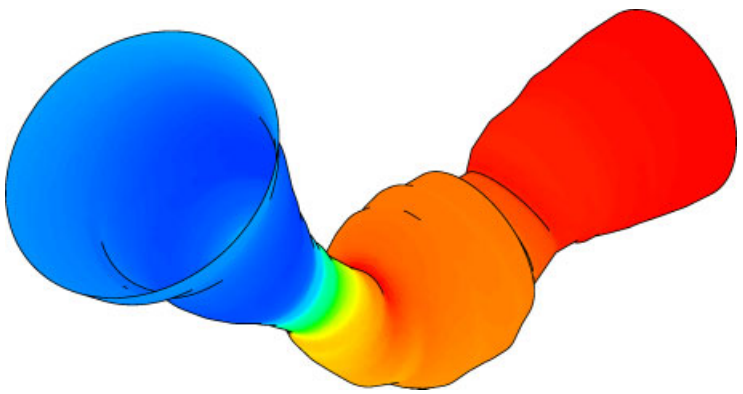

Figure 24. Flow through a model human upper airway. Surface pressure contours near epiglottis.

 

## 10. CONCLUSIONS AND FUTURE RESEARCH

This paper summarized the characteristic-based scheme and its application to the fluid dynamics problems. We believe that the CBS scheme is now well established and being adopted to solve non-fluid dynamics problems. We hope the readers will be able to produce and test their own CBS codes after reading this paper and help further research in this area.

In spite of being tested for many problems of fluid dynamics the CBS scheme needs further investigation in this area to further improve the accuracy of solutions. One of such areas is the development of a better constant-free shock capturing artificial dissipation. Currently employed methods come with a constant to be tuned. At sub- and supersonic flows, this constant is easy to tune and fairly accurate solution is almost always obtained. However, at transonic flows with shocks attached to solid surfaces, this constant is not easy to tune and wrong value may result in a wrong location of the shock. This is often misunderstood previously as the flaw in the CBS scheme. There is definitely a need for a better and constant-free artificial dissipation method.

The second aspect, which needs further investigation is the transient accuracy of the CBS scheme. Although, several transient problems have been tested in the past, we never investigated the effect of 'split' on the transient accuracy. It is known that the projection or split schemes introduce a first-order pressure error into the transient solution. We neither investigated this error in the CBS context nor worked out any way of curbing such error. There are several potential ways to eliminate this error. An obvious possibility would be to use a classical second-order splitting scheme, which retains the pressure term in the momentum equation and evaluates it explicitly. This, however, removes the inherent pressure stability property of the CBS scheme and pressure stability should be restored via other means. The possible strategies to achieve this are use of different velocity–pressure interpolation, which satisfies the LBB condition or use of pressure stabilized formulations as discussed in Reference [66].

The third aspect, which was partially investigated in the past is the use of higher order spatial discretization. In recent times, the linear element was almost adopted universally in the published CBS papers. Further, studies are necessary to shed some light on the advantages of higher order elements in the CBS context.

ACKNOWLEDGEMENTS

The first author acknowledges Ray Hickey's assistance in producing ONERA wing results.

REFERENCES

1. Zienkiewicz OC, Codina R. Search for a general fluid mechanics algorithm. In *Frontiers of Computational Fluid Dynamics*, Caughey DA, Hafez MM (eds). Wiley: New York, 1995; 101–113.
2. Zienkiewicz OC, Codina R. A general algorithm for compressible and incompressible flow—part I: The split, characteristic-based scheme. *International Journal for Numerical Methods in Fluids* 1995; **20**:869–885.
3. Zienkiewicz OC, Taylor RL, Nithiarasu P. *The Finite Element Method for Fluid Dynamics* (6th edn). Elsevier: Amsterdam, 2005.
4. Brooks AN, Hughes TJR. Streamline upwind/Petrov–Galerkin formulation for convection dominated flows with particular emphasis on the incompressible Navier–Stokes equation. *Computer Methods in Applied Mechanics and Engineering* 1982; **32**:199–259.

 

5. Hughes TJR, Mallet M. A new finite element method for computational fluid dynamics: III. The generalized streamline operator for multidimensional advective–diffusive systems. *Computer Methods in Applied Mechanics and Engineering* 1986; **58**:305–328.
6. Hughes TJR, Franca LP, Hulbert GM. A new finite element formulation for computational fluid dynamics: VIII. The Galerkin/least-squares method for advective–diffusive equations. *Computer Methods in Applied Mechanics and Engineering* 1989; **73**:173–189.
7. Onate E. Derivation of stabilized equations for numerical solution of advective–diffusive transport and fluid flow problems. *Computer Methods in Applied Mechanics and Engineering* 1998; **151**:233–265.
8. Hughes TJR. Multiscale phenomena: Green's functions, the Dirichlet-to Neumann formulation, subgrid sale models, bubbles and the origins of stabilized methods. *Computer Methods in Applied Mechanics and Engineering* 1995; **127**:387–401.
9. Codina R. Comparison of some finite element methods for solving the diffusion-convection-reaction equations. *Computer Methods in Applied Mechanics and Engineering* 1998; **156**:185–210.
10. Löhner R, Morgan K, Zienkiewicz OC. The solution of non-linear hyperbolic equation systems by the finite element method. *International Journal for Numerical Methods in Fluids* 1984; **4**:1043–1063.
11. Mortan KW. Generalised Galerkin methods for hyperbolic problems. *Computer Methods in Applied Mechanics and Engineering* 1985; **52**:847–871.
12. Lee JHW, Peraire J, Zienkiewicz OC. The characteristic-Galerkin method for advection-dominated problems—an assessment. *Computer Methods in Applied Mechanics and Engineering* 1987; **61**:359–369.
13. Childs PN, Mortan KW. Characteristic Galerkin methods for scalar conservation laws in one dimension. *SIAM Journal on Numerical Analysis* 1990; **27**:553–594.
14. Pironneau O, Liou J, Tezduyar T. Characteristic-Galerkin and Galerkin/least-squares space-time formulations for the advection–diffusion equation with time-dependent domains. *Computer Methods in Applied Mechanics and Engineering* 1992; **100**:117–141.
15. Donea J, Quartapelle L. An introduction to finite element methods for transient advection problems. *Computer Methods in Applied Mechanics and Engineering* 1992; **95**:169–203.
16. Donea J, Huerta A. *Finite Element Methods for Flow Problems*. Wiley: New York, 2003.
17. Kaazempur-Mofrad MR, Ethier CR. An efficient characteristic Galerkin scheme for the advection equation in 3-D. *Computer Methods in Applied Mechanics and Engineering* 2002; **191**:5345–5363.
18. Kaazempur-Mofrad MR, Minev PD, Ethier CR. A characteristic/finite element algorithm for time-dependent 3-D advection dominated transport using unstructured grids. *Computer Methods in Applied Mechanics and Engineering* 2003; **192**:1281–1298.
19. Zienkiewicz OC, Taylor RL, Zhu JZ. *The Finite Element Method. Its Basis and Fundamentals* (6th edn). Elsevier: Amsterdam, 2005.
20. Chorin AJ. A numerical method for solving incompressible viscous problems. *Journal of Computational Physics* 1967; **2**:12.
21. Zienkiewicz OC, Wu J. A general explicit or semi-explicit algorithm for compressible and incompressible flows. *International Journal for Numerical Methods in Engineering* 1992; **35**:457–479.
22. Zienkiewicz OC, Sai BVKS, Morgan K, Codina R, Vázquez M. A general algorithm for compressible and incompressible flow—part II. Tests on the explicit form. *International Journal for Numerical Methods in Fluids* 1995; **20**:887–913.
23. Codina R, Vázquez M, Zienkiewicz OC. General algorithm for compressible and incompressible flows. Part III—a semi-implicit form. *International Journal for Numerical Methods in Fluids* 1998; **27**:13–32.
24. Zienkiewicz OC, Sai BVKS, Morgan K, Codina R. Split characteristic based semi-implicit algorithm for laminar/turbulent incompressible flows. *International Journal for Numerical Methods in Fluids* 1996; **23**:1–23.
25. Sai BVKS, Zienkiewicz OC, Manzari MT, Lyra PRM, Morgan K. General purpose vs special algorithms for high speed flows with shocks. *International Journal for Numerical Methods in Fluids* 1998; **27**:57–80.
26. Nithiarasu P, Zienkiewicz OC, Sai BVKS, Morgan K, Codina R, Vázquez M. Shock capturing viscosities for the general fluid mechanics algorithm. *International Journal for Numerical Methods in Fluids* 1998; **28**:1325–1353.
27. Massarotti N, Nithiarasu P, Zienkiewicz OC. Characteristic-based-split (CBS) algorithm for incompressible flow problems with heat transfer. *International Journal for Numerical Methods in Fluids* 1998; **8**:969–990.
28. Zienkiewicz OC, Nithiarasu P, Codina R, Vázquez M, Ortiz P. The characteristic based split procedure: an efficient and accurate algorithm for fluid problems. *International Journal for Numerical Methods in Fluids* 1999; **31**:359–392.

 

29. Nithiarasu P, Zienkiewicz OC. On stabilisation of the CBS algorithm. Internal and external time steps. *International Journal for Numerical Methods in Engineering* 2000; **48**:875–880.
30. Zienkiewicz OC, Nithiarasu P. A universal algorithm for fluid dynamics. The Characteristic Based Split (CBS) procedure. Some tests on stability and boundary conditions. *Archives of Mechanics* 2000; **52**: 857–887.
31. Nithiarasu P. On boundary conditions of the CBS algorithm for computational fluid dynamics. *International Journal of Numerical Methods in Engineering* 2002; **54**:523–536.
32. Liu C-B, Nithiarasu P. Incompressible turbulent flow calculations using the explicit characteristic based split (CBS) scheme on unstructured meshes. *European Congress on Computational Methods in Applied Sciences and Engineering ECCOMAS 2004*. Jyvaskyla, 24–28 July 2004.
33. Nithiarasu P, Massarotti N, Mathur JS. Forced convection heat transfer from solder balls on a printed circuit board using the Characteristic Based Split (CBS) scheme. *International Journal of Numerical Methods in Heat and Fluid Flow* 2005; **15**:73–95.
34. Nithiarasu P. An Arbitrary Eulerian Lagrangian (ALE) method for free surface flow calculations using the Characteristic Based Split (CBS) scheme. *International Journal for Numerical Methods in Fluids* 2005; **48**:1415–1428.
35. Nithiarasu P, Liu C-B. An explicit Characteristic Based Split (CBS) scheme for incompressible turbulent flows. *Computer Methods in Applied Mechanics and Engineering* 2006. DOI:10.1016/j.cma.2004.09.017
36. Nithiarasu P, Liu C-B. Steady and unstable flow calculations in a double driven cavity using the explicit CBS scheme. *International Journal for Numerical Methods in Engineering* 2005; **63**:380–397.
37. Zienkiewicz OC, Ortiz P. A split characteristic based finite element model for shallow water equations. *International Journal for Numerical Methods in Fluids* 1995; **20**:1061–1080.
38. Ortiz P, Zienkiewicz OC. Tide and bore propagation in the Severn Estuary by a new algorithm. In *Proceedings of the 9th International Conference of Finite Elements Fluids—New Trends and Applications*. Venezia, October 1995; 1543–1552.
39. Zienkiewicz OC, Rojek J, Taylor RL, Pastor M. Triangles and tetrahedra in explicit dynamic codes for solids. *International Journal for Numerical Methods in Engineering* 1999; **43**:565–583.
40. Massarotti N, Nithiarasu P, Zienkiewicz OC. Natural convection in porous medium—fluid, interface problems. A finite element analysis by using the CBS procedure. *International Journal of Numerical Methods for Heat and Fluid Flow* 2001; **11**:473–490.
41. Massarotti N, Nithiarasu P, Carotenuto A. Microscopic and macroscopic approach for natural convection in enclosures filled with fluid saturated porous medium. *International Journal of Numerical Methods for Heat and FLuid Flow* 2003; **13**:862–886.
42. Nithiarasu P. An efficient artificial compressibility (AC) scheme based on the characteristic based split (CBS) method for incompressible flows. *International Journal for Numerical Methods in Engineering* 2003; **56**:1815–1845.
43. Nithiarasu P, Mathur JS, Weatherill NP, Morgan K. Three-dimensional incompressible flow calculations using the characteristic based split (CBS) scheme. *International Journal for Numerical Methods in Fluids* 2004; **44**:1207–1229.
44. Nithiarasu P. A fully explicit characteristic based split (CBS) scheme for viscoelastic flow calculations. *International Journal for Numerical Methods in Engineering* 2004; **60**:949–978.
45. Codina R, Zienkiewicz OC. CBS versus GLS stabilisation of the incompressible Navier–Stokes equations and the role of the time step as stabilisation parameter. *Communications in Numerical Methods in Engineering* 2002; **18**:99–112.
46. Codina R, Coppola-Owen H, Nithiarasu P, Liu C-B. Numerical comparison of CBS and SGS as stabilisation techniques for the incompressible Navier–Stokes equations. *European Congress on Computational Methods in Applied Sciences and Engineering ECCOMAS 2004*. Jyvaskyla, 24–28 July 2004.
47. Morgan K, Peraire J, Peiro J, Zienkiewicz OC. Adaptive remeshing applied to the solution of a shock interaction problem on a cylindrical leading edge. In *Computational Methods in Aeronautical Fluid Dynamics* Stow P (ed.). Clarenden Press: Oxford, 1990; 327–344.
48. Thomas CG, Nithiarasu P. Effect of variable smoothing and stream line direction on the viscous compressible flow calculations. *International Journal of Numerical Methods for Heat and Fluid Flow* 2005; **15**:420–428.
49. Hirsch C. Numerical computation of internal and external flows. *Fundamentals of Numerical Discretization*, vol. I. Wiley: Chichester, 1988.
50. Pullium TH, Barton JT. Euper computationa of AGARD working group 07, Airfoil test cases, *AIAA 23rd Aerospace Sciences Meeting*. Reno, Naveda, 14–17 January 1986.

 

51. Hassan O, Probert EJ, Morgan K, Peraire J. Mesh generation and adaptivity for the solution of compressible viscous high speed flows. *International Journal for Numerical Methods in Engineering* 1995; **38**:1123–1148.
52. Castro-Diaz MJ, Bourouchaki H, George PL, Hecht F, Mohammadi B. Error interpolation minimization and anisotropic mesh generation. *Proceedings of the International Conference of Finite Elements Fluids—New Trends Applications*. Venezia, 15–21 October 1995; 1139–1148.
53. Castro-Diaz MJ, Bourouchaki H, George PL, Hecht F, Mohammadi B. Anisotropic adaptive mesh generation in two dimensions for CFD. *Computational Fluid Dynamics* 1996; 181–186.
54. Hassan O, Morgan K, Probert J, Peraire J. Unstructured tetrahedral mesh generation for three-dimensional viscous flows. *International Journal for Numerical Methods in Engineering* 1996; **39**:549–576.
55. Borouchaki H, George PL, Hecht F, Laug P, Saltel E. Delaunay mesh generation governed by metric specifications, part I. Algorithms. *Finite Elements Analysis Design* 1997; **25**:61–83.
56. Sorensen KA, Hassan O, Morgan K, Weatherill NP. A multigrid accelerated hybrid unstructured mesh method for 3D compressible turbulent flow. *Computational Mechanics* 2003; **31**:101–114.
57. Venkatakrishnan V. Viscous computations using a direct solver. *Computers and Fluids* 1990; **18**:191–204.
58. Mittal S. Finite element computation of unsteady viscous compressible flows. *Computer Methods in Applied Mechanics and Engineering* 1998; **157**:151–175.
59. Gülçat Ü, Aslan AR. Accurate 3D viscous incompressible flow calculations with FEM. *International Journal for Numerical Methods in Fluids* 1997; **25**:985–1001.
60. Rimon Y, Cheng SI. Numerical solution of a uniform flow over a sphere at intermediate Reynolds numbers. *Physics of Fluids* 1969; **12**:949–959.
61. Gemci T, Corcoran TE, Yakut K, Shortall B, Chigier N. Spray dynamics and deposition of inhaled medications in the throat. *ILASS-Europe 2001*, Zurich, 2–6 September 2001.
62. Li W-I, Edwards DA. Aerosal particle transport and deaggregation phenomena in the mouth and throat. *Advanced Drug Delivery Reviews* 1997; **26**:41–49.
63. Zhang Z, Kleinstreuer C, Kim CS. Computational analysis of micron-particle deposition in a human triple bifurcation airway model. *Computer Methods in Biomechanics and Bimedical Engineering* 2002; **5**:135–147.
64. Kleinstreuer C, Zhang Z. Laminar-to-turbulent fluid-particle flows in human airway model. *International Journal of Multiphase flow* 2003; **29**:271–289.
65. Martonen TB, Zhang Z, Yue G, Musante CJ. 3D particle transport within the human upper respiratory tract. *Aerosol Science* 2002; **33**:1095–1110.
66. Nithiarasu P, Zienkiewicz OC. Analysis of an explicit matrix free fractional step method for incompressible flows. *Computer Methods in Applied Mechanics and Engineering* 2006. DOI:10.1016/j.cma.2005.11.004

 